List of relevant changes

Below is a summary of the main revisions, reflecting the point-by-point responses to the reviewers provided in the following pages.

- Major revisions have been made to the treatment of uncertainties, including the implementation of the Effective Variance Least Squares (EVLS) method within RASPBERRY and chemical PMF. A new section (Sect. 3.3, 'Retrieval uncertainty and RASPBERRY+EVLS') has been added to describe and illustrate the method.
- Based on these new developments, the comparison between RASPBERRY and the chemical PMF has been further expanded using multiple regression approaches.
- Additional explanations have been included to further clarify the RASPBERRY methodology and to enhance the reproducibility of the selection of uncertainty parameters.
- A discussion of the measurement uncertainty associated with the OPC used in the study has been added.
- The discussion of the obtained aerosol source profiles has been expanded, including a more comprehensive comparison with existing literature data.
- Figures and captions have been improved to enhance readability and interpretation, with additional clarification where required.
- Technical corrections and refinements have been implemented in response to specific reviewer comments (e.g. terminology, references, and methodological details).

To preserve the readability and narrative flow of the main text, more extensive additions and detailed discussions have been included in the Supplementary Material.

Overall, we believe that the revisions have strengthened the manuscript and adequately addressed all reviewer comments.

Response to Referee #1

We thank the reviewer for his/her time and consideration, and for the constructive comments. We are confident that all remarks have been carefully addressed and that the manuscript has been improved accordingly. Our point-by-point response is provided below (text in italics denotes excerpts from the revised manuscript).

Referee's comment 1. Diémoz et al. presents a new PM10 source apportionment framework, RASPBERRY, based on aerosol physical properties derived from OPC and aethalometer measurements. By comparison with chemical PMF results, the authors showed the clear strengths of RASPBERRY. The manuscript is well organized and easy to follow. However, I still have some issues before the manuscript can be accepted. Line 292, the authors mentioned "heuristic uncertainty" was optimized through trial-error methods or iterative approach. Given the strong influence of uncertainty definition of PMF outcomes, can authors provide more details how to derive this parameterization to ensure the reproductivity?

Author's response 1. We thank the reviewer for the positive overall assessment and for raising the point of the limited level of detail originally provided to describe the uncertainty configuration in our approach. Indeed, RASPBERRY reproductivity is actually a goal of this work. To address this potential shortcoming, while at the same time keeping the main text concise, we expanded Sect. S7 of the Supplement. In particular, we now provide a complete description of the procedure used to determine the optimal uncertainty configuration. This workflow is presented in an objective and reproducible manner. We also removed the term 'heuristic', which – although commonly used in the PMF literature – may give the misleading impression that the parameter selection was excessively subjective or arbitrary.

The revised text reads:

The uncertainty framework employed in this study follows the methodology outlined by Vörösmarty et al. (2024), in which the PMF input uncertainty is parametrised as in Eqs. (4) and (5) of the main text. This formulation essentially represents a semi-empirical error model, with notation likely inherited from earlier PMF implementations (PMF2), and separates the uncertainty into two components representing common sources of uncertainty in aerosol measurements: (i) baseline instrument/analysis noise, ensuring a minimum uncertainty even when concentrations are small; and (ii) a concentration-dependent error, which increases proportionally with the measured concentration. The interested reader is referred to that work, and the references therein, for further details. Here we instead present an objective and reproducible workflow describing, step by step, how the free coefficients A, α, and C_3 were selected:

1. *Choice for A and α started from relevant ranges suggested in the aforementioned study and in the scientific literature (e.g., Zhou et al., 2005a; Ogulei et al., 2006, 2007; Gu et al., 2011), i.e. 0.01 to 0.05*

for the product $A \times \alpha$. In our case, $A = 1$ was assigned to size channels and optical absorption, and $\alpha = 0.01$ was used as an initial value, following Vörösmarty et al. (2024).

2. *Choice for C_3 started from values between 0.01 and 0.5. For example, Vörösmarty et al. (2024) select 0.10 for most of their channels. A value of 10 % represents a reasonable a priori estimate of the uncertainty when no additional information is available, therefore C_3 was initially set to this value in our case.*

3. *We then ensured that the total variable (e.g., PM_{10}) did not influence the factorisation by setting it as 'weak' in the PMF (or by assigning $A = 3$ and $C_3' = C_3 \times 3$).*

4. *An initial PMF run was performed, and the residual distribution (Q/Q_{exp}) for each 'species' (VSD channels from OPC and aethalometer spectral absorption at the measured wavelengths) was recorded. At this stage, the volume distribution component typically dominated the profile splitting and was better reproduced by the PMF, with the exception of the largest size ranges (as also reported by Vörösmarty et al., 2024), whereas spectral absorption contributed only marginally to the separation and was not well reproduced (resulting in a high Q/Q_{exp} ratio). This behaviour arises from the larger number of 'channels' associated with particle size (OPC measurements) compared with those related to multispectral optical absorption (aethalometer). This imbalance was corrected in the subsequent steps.*

5. *We gradually adjusted the uncertainty until three criteria were simultaneously satisfied: (i) the factor contributions remained as uncorrelated as possible; (ii) the scaled residuals fell within the expected range (± 3, Norris et al., 2014); and (iii) the resulting profiles and contributions were physically plausible.*

6. *In our case, reducing the residuals (and the Q/Q_{exp} ratio) for the largest size channels without artificially splitting the coarse 'local resuspension' factor into two modes required increasing their uncertainty. This resulted in $C_3 = 0.3$ for size channels with particles larger than $2\,\mu m$ and $C_3 = 0.4$ for particles above $6\,\mu m$. The $2\,\mu m$ and $6\,\mu m$ thresholds were selected as representative of the desert dust and coarse resuspension modes, based on previous literature (see main text) and the examination of the temporal evolution of the volume size distributions. Indeed, these C_3 values improved the separation between desert dust and local resuspension contributions. Larger uncertainty values tended to merge these contributions, whereas smaller values tended to split the local resuspension factor into multiple modes.*

7. *Conversely, in order for the absorption measurements to contribute effectively to shaping the factor profiles, their uncertainty had to be reduced. In this study, C_3 was set to 0.05 for aethalometer measurements. Using higher values caused the size-related portion of the PMF to dominate due to the larger number of size classes, leading to additional size modes lacking clear physical interpretation. In some configurations, the contributions associated with traffic emissions and residential biomass burning became unrealistically small. Similar issues concerning the mass of the traffic factor were reported by Forello et al. (2023). Notably, the selected configuration yielded PM_{10} contributions for traffic and biomass burning that are consistent with the method described by Aujay-Plouzeau (2020), which is based solely on aethalometer measurements.*

8. *During this process, it was necessary to increase the number of factors relative to the initial run, which was based only on size, in order to accommodate factors emerging from the multispectral absorption-driven splitting (e.g., traffic, biomass burning, condensation-mode secondary aerosols). More details on the selection of the optimal number of factors are provided in Sect. S11.*

9. *The plot of the original and reconstructed time series were examined for each input species to verify whether the selected uncertainty configuration reproduced the original data satisfactorily.*

10. *Note that α primarily affects the PMF behaviour at low concentrations of a species, whereas C_3 influences the behaviour at medium to high concentrations. This distinction is particularly important for species exhibiting a marked seasonal cycle, such as those related to biomass burning. In such cases, the minimum uncertainty (constant component, see Table S1) should be chosen so that winter and summer conditions are clearly distinguished, i.e. situations in which the species is present or absent in the atmosphere are well separated.*

11. *The factor uncertainties were finely adjusted at the end of the procedure by scaling them so that the residuals fell within the expected range of* ± 3. *In this study, an additional 20 % increase in all* C_3 *values was required. The coefficients were scaled accordingly rather than introducing an additional parameter ('Additional model uncertainty') in EPA PMF 5.0. The* C_3 *values reported in Table S1 include this factor and their reported digits are approximated to* ± 0.05 *for clarity.*

The final values for the parameters A, α*, and* C_3 *are shown in Table S1. [...]*

It may be noted that:

- *The uncertainty assigned to the largest size channels (*$d > 6\,\mu m$*) is relatively high. This reflects the low number concentration of large particles and their 'shot' nature, which introduces greater variability when considered from a Poisson-based perspective (Sect. S2.1). Indeed, these bins typically contain a few peak values emerging from a background of zeros, whose frequency can reach up to 30 %. Consequently, these size channels, together with the total variable* PM_{10}*, were classified as weak variables in the PMF configuration to prevent them from exerting excessive influence during subsequent tests. During the testing phase, as suggested in previous studies (e.g., Zhou et al., 2004; Thimmaiah et al., 2009; Zhou et al., 2005b), an alternative approach was also evaluated in which the largest size bins were grouped (in sets of three to five, depending on particle size) to mitigate issues associated with low particle counts and to improve the signal-to-noise ratio (SNR). Although bin grouping effectively increased the SNR, it hindered the separation of the two coarse factors (desert dust and local resuspension). For this reason, this approach was not adopted in the final configuration.*
- *The NeBC uncertainties used in this study are lower than those reported in some previous works (e.g., Forello et al., 2019; Rigler et al., 2020). In particular, Forello et al. (2023) applied an uncertainty as high as 50 % for* b_{abs} *to avoid convergence issues when coupling absorption data with chemical data in the PMF. With such high uncertainty values, combined with the smaller number of optical variables relative to chemical species, the NeBC information effectively follows the factorisation rather than contributing to it. In contrast, the present approach aims to ensure that both spectral absorption and volume size distribution contribute to determining the final solution. Consequently, the uncertainty values adopted here should not be interpreted as strict measurement uncertainties, but rather as weighting parameters used to balance the influence of the different input variables on the Q metric.*

RC2. For traffic emissions between chemical and physical PMF results, their correlation is not that high, r2=0.45. The authors attributed to the detection limit of OPC. Is it possible to improve the physical PMF by introducing other factors, such as NOx?

AR2. We thank the reviewer for this comment, which allowed us to clarify the reasons why NO_x were not included in the PMF. More specifically, we introduced the following section in the Supplement (Sect. S5: On the inclusion of gases in the physical PMF):

Recent guidelines of the European project RI-URBANS (Petit et al., 2024) also suggest including NO_x *in PMF analyses. This practice may be useful for supporting the factor-source attribution based on the factor* NO_x *is associated with. In such cases,* NO_x *should be introduced into the PMF as weak species (e.g., Vörösmarty et al., 2024) in order to prevent them from exerting an excessive influence on the separation of the factors (see below).*

However, it should be considered that in Alpine environments, particularly during winter, NO_x *does not exclusively trace traffic emissions but also biomass combustion, and that Aosta is a relatively small, low-traffic city (33,000 inhabitants; Diémoz et al., 2019, 2020, 2021). In the chemical PMF, for example, the*

correlation of NO, NO_2, and NO_x with the biomass-burning factor is higher (R^2 = 0.63, 0.63, and 0.67, respectively) than with the traffic factor (R^2 = 0.56, 0.45, and 0.53).

For this reason, we were cautious about using NO_x as a strong species contributing to the separation of the factors. Several tests performed during the development of this work indicate that, when NO_x is introduced as a strong species, the agreement between the chemical and physical PMF deteriorates and, in some cases, the physical PMF yields unrealistic solutions. For example:

- *When NO_x is introduced with an uncertainty of 5–10 %, the seasonal cycle of NO_x is poorly reproduced by the PMF, with NO being strongly underestimated during winter.*
- *When the uncertainty assigned to NO_x is reduced, both NO and NO_2 are forced to be reproduced more accurately. However, the reconstruction of DeltaC deteriorates ($Q/Q_{exp} = 20$), and the contributions of PM_{bb} and PM_{ff} decrease by approximately a factor of three (i.e., to ~3 %). In some configurations, an additional NO-rich factor separates from the factor associated with traffic emissions.*

This behaviour is likely related to the fact that the relationship between NO_x and aerosol, as also discussed by Rivas et al. (2020), depends on several factors: (a) meteorology and atmospheric dynamics (e.g. solar radiation availability, temperature, etc.); (b) long-term changes in the vehicle fleet; and (c) driving conditions. Consequently, the ratio between NO_x and traffic-related PM can vary throughout the day, between seasons, and over longer time scales as the ones addressed here. In addition, if as we expect the exhaust fraction is not fully captured by the OPC and the PMF is forced to maintain a strong correlation with NO_x, the model may compensate this constraint by reducing the PM_{10} mass attributed to traffic.

Moreover, taking the suggestions received in the review process into account, we introduced the calculation of the uncertainties of the factor contributions (matrix G) for each retrieval using the Effective Variance Least Squares (EVLS) method coupled to the chemical PMF and RASPBERRY. With respect to the traffic factor, this analysis clearly shows that traffic is the factor associated with the largest relative uncertainties, both in the chemical PMF and in RASPBERRY+EVLS. This combination of low signal and comparatively large uncertainty naturally leads to a substantial dispersion in the point-to-point comparison (Fig. 1 here, complementing the results in Fig. 8b reported in the first version of the manuscript and now included in Fig. S34).

We included this discussion in the revised manuscript, and the corresponding paragraph in Sect. 4.3 was therefore updated as follows:

The comparison of traffic factors is depicted in Figs. 8a (time series) and 8b (scatter plot). From the first panel, it is evident that the magnitude of contributions from both source apportionments is about the same, as are the overall seasonal trends. However, the point-to-point relationship illustrated in the second panel reveals some discrepancies, with a Pearson's correlation coefficient of $\rho = 0.67$ (R^2 = 0.45). Furthermore, the regression coefficients deviate from the 1:1 line ($y = 0.58\,x + 0.72\ \mu g\,m^{-3}$). This deviation can be attributed to difficulties in accurately identifying the traffic factor, primarily due to the following reasons:

- *Contributions from both source apportionments are relatively low, steadily remaining below 6 $\mu g\,m^{-3}$, which is consistent with the fact that Aosta is a relatively small, low-traffic city (33,000 inhabitants; Diémoz et al., 2019, 2020, 2021). At the same time, the relative uncertainty associated with traffic emissions is among the highest of all dimensional profiles. This is evident from both the large interval ratio obtained from the DISP test (Sect. 4.2 and Fig. 3) and from the uncertainties derived using the EVLS method for both the physical and the chemical data sets (Fig. S34).*
- *The finite lower detection limit of the OPC does not allow all aerosols emitted by traffic to be captured. In particular, most of the studies focusing on ultrafine and accumulation-mode particles (among the most recent examples, Harni et al., 2024; Beddows et al., 2025; Ćirović et al., 2026; Mapelli et al., 2026) identified at least two distinct factors related to traffic (e.g., freshly nucleated vs more aged or distant particles, or gasoline vs diesel/heavy-duty emissions). This may indicate that the physical setup and the chemical analyses effectively 'detect' different factors attributed to traffic.*

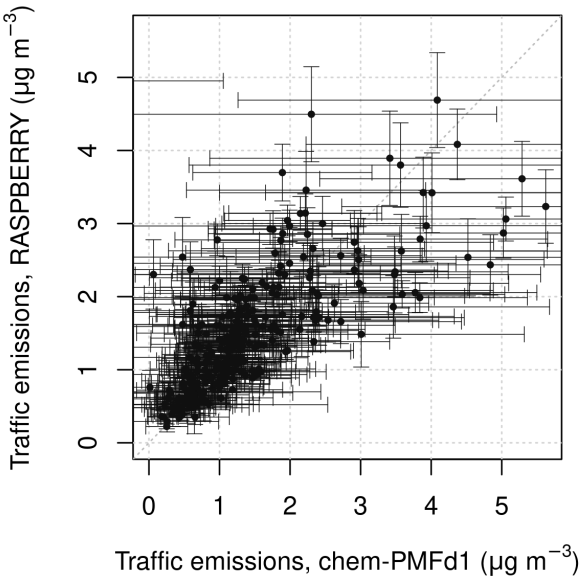

Figure 1: Comparison of daily-averaged PM_{10} source contributions attributed to traffic derived from the chemical PMF (further reprocessed using EVLS) and RASPBERRY+EVLS, shown together with their individual uncertainties. The figure clearly shows that the uncertainty in the chemical source apportionment is larger than in the physical one.

- *The coarse resuspended fraction, which significantly contributes to the mass, may be characterised in slightly different amounts in the chemical and the physical source apportionments, as discussed in Sect. S10. Distinguishing unambiguously exhaust and non-exhaust particle contributions is a well-known challenge, frequently reported in the literature (Forello et al., 2023).*
- *The mass absorption cross-section (MAC) in aethalometer measurements may decrease in winter compared to summer, as observed in several studies, e.g. Mousavi et al. (2019) in Milan and Savadkoohi et al. (2024) on a European scale. Such seasonal variation is consistent with an underestimation of NeBC during winter, when concentrations are higher, and an overestimation during summer, when concentrations are lower, in RASPBERRY.*

At the same time, it should be noted that the comparison slope for the traffic factor is higher than 1 when using York and log-transformed York regressions (Table S3), since the intercept decreases. Therefore, the deviation from the 1:1 line may also be partly attributable to an artefact of the regression method itself.

RC3. The authors also mentioned RASPBERRY improves the efficiency of PMF. How much faster is RASPBERRY is compared to a normal PMF? Can we also apply RASPBERY to the chemical PMF? If so, it would be helpful to discuss whether and how the results would differ from those obtained using a normal chemical PMF approach.

AR3. As shown in Fig. S7, when RASPBERRY retrievals are performed on the same input data, and using the same uncertainties/profiles from the training phase (PMF), the contributions from RASPBERRY and the 'standard' PMF are equivalent. This follows from the fact that the same metric is minimised during both the training and the retrieval phases (Eq. 3), regardless of the dataset used. In principle, the same methodology could also be applied to chemical datasets, in a way conceptually similar to what is commonly known in the literature as the Chemical Mass Balance (CMB) approach. It should also be noted

that, for source apportionment based on online aerosol chemical characterisation measurements, more sophisticated tools than RASPBERRY are available, such as SoFi (Canonaco et al., 2013).

The retrieval phase of RASPBERRY is typically one to two orders of magnitude faster than the PMF training phase for the same number of observations. However, since chemical analyses are generally performed offline on daily samples, the number of data points to be processed is usually much smaller than for physical measurements, which are typically automatic and collected at high time resolution. Consequently, from the perspective of data volume, the computational advantage of applying RASPBERRY to chemical datasets would likely be smaller than that demonstrated in this work for physical measurements. Conversely, once the training phase has been completed, RASPBERRY can be applied to real-time physics-based measurements, enabling rapid source apportionment while avoiding delays associated with PM sampling and chemical analyses, as well as the need to collect sufficiently long-term datasets to perform a chemical PMF. Therefore, RASPBERRY allows environmental agencies to conduct high temporal resolution, real-time, continuous, and cost-effective aerosol source apportionment, while also supporting emergency management.

References

Aujay-Plouzeau, R.: Guide méthodologique pour la mesure du «Black Carbon» par Aethalomètre multi longueur d'onde AE33 dans l'air ambiant (Version 2020), Tech. rep., Ineris, https://www.lcsqa.org/system/files/media/documents/LCSQA2019-Guide_mesure_BlackCarbon_par_AE33_VF03-Approuv%C3%A9CPS15122020.pdf, 2020.

Beddows, D., Brean, J., Rowell, A., Merkel, M., Weinhold, K., Dall'Osto, M., and Harrison, R.: Wide-Positive Matrix Factorisation of particle number size distributions: A new approach accounting for cyclically changing source profiles, Sci. Total Environ., 998, 180 231, https://doi.org/10.1016/j.scitotenv.2025.180231, 2025.

Canonaco, F., Crippa, M., Slowik, J. G., Baltensperger, U., and Prévôt, A. S. H.: SoFi, an IGOR-based interface for the efficient use of the generalized multilinear engine (ME-2) for the source apportionment: ME-2 application to aerosol mass spectrometer data, Atmos. Meas. Tech., 6, 3649–3661, https://doi.org/10.5194/amt-6-3649-2013, 2013.

Ćirović, Ž., Stojanović, D. B., Davidović, M., Onjia, A., Alastuey, A., and Jovašević-Stojanović, M.: New Particle Formation and Source Apportionment of Particle Number Size Distribution in the Urban Area of the City of Belgrade, Atmosphere, 17, https://doi.org/10.3390/atmos17020205, 2026.

Diémoz, H., Gobbi, G. P., Magri, T., Pession, G., Pittavino, S., Tombolato, I. K. F., Campanelli, M., and Barnaba, F.: Transport of Po Valley aerosol pollution to the northwestern Alps – Part 2: Long-term impact on air quality, Atmos. Chem. Phys., 19, 10 129–10 160, https://doi.org/10.5194/acp-19-10129-2019, 2019.

Diémoz, H., Tombolato, I. K. F., Zublena, M., Magri, T., and Ferrero, L.: The impact of biomass burning emissions on PM concentration in the Greater Alpine region, in: Proceedings of 12th International Conference on Air Quality, Science and Application, p. 26, Hatfield, UK, 10.18745/pb.22217, 2020.

Diémoz, H., Magri, T., Pession, G., Tarricone, C., Tombolato, I. K. F., Fasano, G., and Zublena, M.: Air Quality in the Italian Northwestern Alps during Year 2020: Assessment of the COVID-19 «Lockdown Effect» from Multi-Technique Observations and Models, Atmosphere, 12, https://doi.org/10.3390/atmos12081006, 2021.

Forello, A. C., Bernardoni, V., Calzolai, G., Lucarelli, F., Massabò, D., Nava, S., Pileci, R. E., Prati, P., Valentini, S., Valli, G., and Vecchi, R.: Exploiting multi-wavelength aerosol absorption coefficients in a multi-time resolution source apportionment study to retrieve source-dependent absorption parameters, Atmos. Chem. Phys., 19, 11 235–11 252, https://doi.org/10.5194/acp-19-11235-2019, 2019.

Forello, A. C., Cunha-Lopes, I., Almeida, S. M., Alves, C. A., Tchepel, O., Crova, F., and Vecchi, R.: Insights on the combination of off-line and on-line measurement approaches for source apportionment studies, Sci. Total Environ., 900, 165 860, https://doi.org/10.1016/j.scitotenv.2023.165860, 2023.

Gu, J., Pitz, M., Schnelle-Kreis, J., Diemer, J., Reller, A., Zimmermann, R., Soentgen, J., Stoelzel, M., Wichmann, H.-E., Peters, A., and Cyrys, J.: Source apportionment of ambient particles: Comparison of positive matrix factorization analysis applied to particle size distribution and chemical composition data, Atmos. Environ., 45, 1849–1857, https://doi.org/10.1016/j.atmosenv.2011.01.009, 2011.

Harni, S. D., Aurela, M., Saarikoski, S., Niemi, J. V., Portin, H., Manninen, H., Leinonen, V., Aalto, P., Hopke, P. K., Petäjä, T., Rönkkö, T., and Timonen, H.: Source apportionment of particle number size distribution at the street canyon and urban background sites, Atmos. Chem. Phys., 24, 12 143–12 160, https://doi.org/10.5194/acp-24-12143-2024, 2024.

Mapelli, C., Diémoz, H., Contini, D., Dinoi, A., Cesari, D., and Barnaba, F.: Physics-based aerosol source apportionment at the site of Lecce (Italy), Atmos. Res. (under review), 2026.

Mousavi, A., Sowlat, M. H., Lovett, C., Rauber, M., Szidat, S., Boffi, R., Borgini, A., De Marco, C., Ruprecht, A. A., and Sioutas, C.: Source apportionment of black carbon (BC) from fossil fuel and biomass burning in metropolitan Milan, Italy, Atmos. Environ., 203, 252–261, https://doi.org/10.1016/j.atmosenv.2019.02.009, 2019.

Norris, G., Duvall, R., and Brown, S.: EPA Positive Matrix Factorization (PMF) 5.0 Fundamentals and User Guide, U.S. Environmental Protection Agency Office of Research and Development Washington, DC 20460, `https://www.epa.gov/sites/default/files/2015-02/documents/pmf_5.0_user_guide.pdf`, ePA/600/R-14/108, 2014.

Ogulei, D., Hopke, P. K., Zhou, L., Pancras, J. P., Nair, N., and Ondov, J. M.: Source apportionment of Baltimore aerosol from combined size distribution and chemical composition data, Atmos. Environ., 40, 396–410, https://doi.org/10.1016/j.atmosenv.2005.11.075, 2006.

Ogulei, D., Hopke, P. K., Chalupa, D. C., , and Utell, M. J.: Modeling Source Contributions to Submicron Particle Number Concentrations Measured in Rochester, New York, Aerosol Sci. Tech., 41, 179–201, https://doi.org/10.1080/02786820601116012, 2007.

Petit, J.-E., Favez, O., and Chauvigné, A.: Deliverable D5 (D1.5) NRT Source Apportionment Service Tools for submicron carbonaceous matter (final), Tech. rep., RI-URBANS Research Infrastructures Services Reinforcing Air Quality Monitoring Capacities in European Urban & Industrial AreaS (GA n. 101036245), `https://riurbans.eu/wp-content/uploads/2024/12/RI-URBANS_D5_D1_5.pdf`, 2024.

Rigler, M., Drinovec, L., Lavrič, G., Vlachou, A., Prévôt, A. S. H., Jaffrezo, J. L., Stavroulas, I., Sciare, J., Burger, J., Kranjc, I., Turšič, J., Hansen, A. D. A., and Močnik, G.: The new instrument using a TC–BC (total carbon–black carbon) method for the online measurement of carbonaceous aerosols, Atmos. Meas. Tech., 13, 4333–4351, https://doi.org/10.5194/amt-13-4333-2020, 2020.

Rivas, I., Beddows, D. C., Amato, F., Green, D. C., Järvi, L., Hueglin, C., Reche, C., Timonen, H., Fuller, G. W., Niemi, J. V., Pérez, N., Aurela, M., Hopke, P. K., Alastuey, A., Kulmala, M., Harrison, R. M., Querol, X., and Kelly, F. J.: Source apportionment of particle number size distribution in urban background and traffic stations in four European cities, Environ. Int., 135, 105 345, https://doi.org/10.1016/j.envint.2019.105345, 2020.

Savadkoohi, M., Pandolfi, M., Favez, O., Putaud, J.-P., Eleftheriadis, K., Fiebig, M., Hopke, P. K., Laj, P., Wiedensohler, A., Alados-Arboledas, L., Bastian, S., Chazeau, B., Álvaro Clemente María, Colombi, C., Costabile, F., Green, D. C., Hueglin, C., Liakakou, E., Luoma, K., Listrani, S., Mihalopoulos, N., Marchand, N., Močnik, G., Niemi, J. V., Ondráček, J., Petit, J.-E., Rattigan, O. V., Reche, C., Timonen, H., Titos, G., Tremper, A. H., Vratolis, S., Vodička, P., Funes, E. Y., Zíková, N., Harrison, R. M., Petäjä, T., Alastuey, A., and Querol, X.: Recommendations for reporting equivalent black carbon (eBC) mass concentrations based on long-term pan-European in-situ observations, Environ. Int., 185, 108 553, https://doi.org/10.1016/j.envint.2024.108553, 2024.

Thimmaiah, D., Hovorka, J., and Hopke, P. K.: Source apportionment of winter submicron prague aerosols from combined particle number size distribution and gaseous composition data, Aerosol Air Qual. Res., 9, 209–236, https://doi.org/10.4209/aaqr.2008.11.0055, 2009.

Vörösmarty, M., Hopke, P. K., and Salma, I.: Attribution of aerosol particle number size distributions to main sources using an 11-year urban dataset, Atmos. Chem. Phys., 24, 5695–5712, https://doi.org/10.5194/acp-24-5695-2024, 2024.

Zhou, L., Hopke, P. K., Paatero, P., Ondov, J. M., Pancras, J., Pekney, N. J., and Davidson, C. I.: Advanced factor analysis for multiple time resolution aerosol composition data, Atmos. Environ., 38, 4909–4920, https://doi.org/10.1016/j.atmosenv.2004.05.040, 2004.

Zhou, L., Hopke, P. K., Stanier, C. O., Pandis, S. N., Ondov, J. M., and Pancras, J. P.: Investigation of the relationship between chemical composition and size distribution of airborne particles by partial least squares and positive matrix factorization, J. Geophys. Res., 110, https://doi.org/10.1029/2004JD005050, 2005a.

Zhou, L., Kim, E., Hopke, P. K., Stanier, C., and Pandis, S. N.: Mining airborne particulate size distribution data by positive matrix factorization, J. Geophys. Res., 110, https://doi.org/10.1029/2004JD004707, 2005b.

Response to Referee #2

We thank the reviewer for his/her time and consideration, and for the constructive comments. We are confident that all remarks have been carefully addressed and that the manuscript has been improved accordingly. Our point-by-point response is provided below (text in italics denotes excerpts from the revised manuscript).

Referee's comment 1. The authors reported in detail the new PM10 source apportionment approach called RASPBERRY that combined OPC-based particle size distribution and spectrally resolved light absorption. Specifically, the manuscript includes inter-comparison between this physical-based PMF and the commonly used chemical PMF in addition to specific case studies across the Po Valley over the period of 2020-2024. Overall, the paper is well-written with occasional repeated information between figure captions and the main text.

Author's response 1. We thank the reviewer for the positive overall assessment. The text in the figure captions has been shortened where possible, while ensuring that each figure can be understood by the reader without the need to consult additional information in the main text. In particular, the captions of Figs. 3, 7, 8, and 12 have been revised.

RC2. The similar inter-comparison between chemical-PMF and this physical-based analysis is very interesting. One of my main concerns is the lack of uncertainty estimates on some of these comparisons. This manuscript would benefit from a major revision that I hope will address my questions and comments below.

AR2. We thank the reviewer for this comment. In response to this suggestion, major revisions have been made to the discussion of uncertainties. In particular, the manuscript has been significantly expanded by incorporating the application of the Effective Variance Least Squares (EVLS) method to RASPBERRY, as well as to the chemical PMF. This method enables the measurement uncertainties of the input data to be fully propagated into the retrievals, together with the uncertainty associated with rotational ambiguity in the profiles. The method is now illustrated and discussed in the revised manuscript. To this end, a new section (*3.3 Retrieval uncertainty and 'RASPBERRY+EVLS'*) has been introduced:

Conventional PMF analysis as implemented in EPA PMF software yields uncertainties associated with the profile matrix, **F***, but not with the contribution matrix,* **G** *(Paatero et al., 2014). To our knowledge, the evaluation of uncertainties in source contributions remains a debated topic in the scientific literature,*

and no methodology has yet been universally accepted and implemented by the community. As a direct consequence, RASPBERRY does not directly provide uncertainty estimates for the source-apportioned PM_{10} retrievals. Based on common practice and the state-of-the-art literature, however, we propose two approaches to address this limitation.

A first and simpler method consists of propagating the uncertainty from the PMF-derived profiles based on the $dQ^{max} = 4$ range of the DISP test, i.e. the range associated with a maximum increase of 4 in the objective function Q (Eq. 3). This range, often referred to as the 'interval ratio' in the literature (Brown et al., 2015), is commonly used as a proxy for rotational uncertainty in PMF profiles (e.g., Paatero et al., 2014; Masiol et al., 2017). Within this framework, the same relative interval ratio associated to the PM_{10} component of a given profile is also assigned to the contributions of the corresponding factor. For the sake of simplicity, this method is selected to provide an estimate of the uncertainty range in the figures presented in the main text.

The second, more comprehensive method allows not only the propagation of uncertainties associated with the factor profiles but also with the uncertainties in the PMF input species concentrations. This approach is based on the effective variance least squares (EVLS) technique (Watson et al., 1984; Chen et al., 2025), which is also currently implemented in the EPA CMB model (Coulter, 2004). Derived from maximum likelihood theory and successfully validated against the Monte Carlo method (Watson et al., 1984), this technique minimises, through an iterative scheme, a modified Q' metric (slightly different from that used in PMF) that accounts for uncertainties in both receptor concentrations and source profiles. In the present study, following the approach of Chen et al. (2025), the profile uncertainties are derived from the displacement intervals of all species in a profile. Individual uncertainties in the estimated source contributions for each retrieval are subsequently derived by propagation through the covariance matrix of the inversion. We refer to this approach as 'RASPBERRY+EVLS'. The interested reader will find further methodological details and a comparison with RASPBERRY in Sect. S9.

See also our reply #17 in this document, which discusses how the inclusion of uncertainties in RASPBERRY and in the chemical PMF affects the regression coefficients.

RC3. Specific comments/questions: Abstract: The particle size detection limit should be specified when the authors mentioned particle size distribution (L4) (Dp > 0.18 um).

AR3. The abstract was updated as follows: *This study introduces a novel PM_{10} source apportionment approach [...] based on the analysis of aerosol physical properties, namely particle size distributions in the accumulation and coarse modes (D_p in the range 0.18–18 μm) and spectrally resolved light absorption (wavelengths 370–950* nm*).*

RC4. The lack of detection of nucleation and Aitken mode particles has implication (e.g., missing fresh emission).

AR4. Thank you for raising this important issue. We agree with the reviewer regarding the relevance of both nucleation and Aitken modes. At the same time, it is important to clarify the purpose of the RASPBERRY development, the context of its application, and its potential future developments.

Indeed, the lower detection limit of the OPC does not allow a focus on ultrafine particles, as done in other studies that have identified freshly nucleated besides more aged or distant particles, for example in the context of traffic-related sources (among the most recent examples, Harni et al., 2024; Beddows et al., 2025; Ćirović et al., 2026; Mapelli et al., 2026). However, RASPBERRY is designed for PM_{10} *mass*

concentration source apportionment, and the contribution of ultrafine particles to the overall mass is generally negligible. Within this framework, RASPBERRY enables high-temporal-resolution, real-time, continuous, and cost-effective aerosol source apportionment, also supporting emergency management applications. It therefore represents a robust and practical tool that can be applied at any monitoring site equipped at least with an OPC and an aethalometer. The inclusion of ultrafine particle number size distributions would certainly enhance the applicability of the method, for example at ACTRIS sites, but it would also reduce the number of monitoring stations where the approach could be implemented.

Incidentally, the extension of RASPBERRY to include ultrafine particles will be the subject of a separate publication currently under review (Mapelli et al., 2026).

Based on the reviewer's comment, we have modified the abstract as follows: *The availability of such measurements at high temporal resolution enables aerosol* mass *source apportionment from real time to long-term scales. [...] Although demonstrated at a single site, RASPBERRY is readily transferable to international air quality networks* concerned with aerosol mass source apportionment, *as it relies on optical instruments commonly employed by regulatory authorities and environmental protection agencies.*

This limitation is also acknowledge in Sect. 4.3 'Comparison between chemical PMF and physical source apportionment': *The finite lower detection limit of the OPC does not allow all aerosols emitted by traffic to be captured. In particular, most of the studies focusing on ultrafine and accumulation-mode particles (among the most recent examples, Harni et al., 2024; Beddows et al., 2025; Ćirović et al., 2026; Mapelli et al., 2026) identified at least two distinct factors related to traffic (e.g., freshly nucleated vs more aged or distant particles, or gasoline vs diesel/heavy-duty emissions). [...]*

RC5. For the light absorption, the authors should also include the measurement wavelengths for this analysis (370-950 nm).

AR5. Following the reviewer's suggestion, the information has now been included in the abstract, see Author Response #3.

RC6. L127: 'foehr': Is that a typo?

AR6. The word was correctly spelled as 'Foehn' winds. The main text has nevertheless been updated to include a brief explanation: *Foehn winds, i.e. adiabatically warmed lee-side downslope winds associated with orographic precipitation and rain-shadow effects.*

RC7. L142: "all measurements were averaged to a common temporal resolution of 1 hour" – for long term diurnal or seasonal trends I can see that this time averaging is good enough. But for point source emissions like fresh smoke, 1-hr average may be too long. I guess since the particle size measurements do not extend to small particles, the current equipment setup is incapable of capturing these short-term events. Is there any concern about diluting short burst of emissions due to this long time averaging? Or have the authors looked at 30-s or 5-min average of size distributions to ensure they are not missing any point source emissions?

AR7. In the present study, we mainly focused on sources influencing PM_{10} at temporal and spatial scales representative of the urban background rather than on individual point-source emissions. Moreover, unlike many studies in the literature that focus on relatively short observation periods, our analysis covers several years of measurements. This implies handling millions of data points already at an hourly resolution. These considerations led us to adopt 1 h as the optimal averaging period for the measurements, and therefore we did not specifically investigate shorter temporal resolutions, although this could certainly be beneficial for some applications.

In principle, the RASPBERRY algorithm can be applied to data at any temporal resolution, including 30 s or 5 min averages. With sufficient statistical robustness, this could potentially allow the identification of additional factors. In practice, however, excessively short averaging periods may lead to larger measurement uncertainties. This limitation affects both spectral absorption measurements – since the aethalometer relies on a differential measurement principle – and particle size distributions. The latter is particularly critical for coarse particles, which dominate the PM_{10} mass but are present at relatively low number concentrations. In this regime, Poisson counting statistics lead to large relative uncertainties (see Author Response AR#8 and Sect. S2.1). At the measurement site considered in this study, the use of very short averaging times would therefore primarily result in increased noise, without a commensurate gain in information content. Moreover, it may lead to physically implausible artefacts, such as negative NeBC concentration values.

Nevertheless, the reviewer is correct that, in the case of ultrafine particle measurements and studies specifically targeting short-lived emission bursts, the temporal resolution should indeed be shorter than 1 h.

Section S4 has been updated as follows: [...] aethalometer measurements were averaged to 1-hour intervals, and data from all instruments in Aosta–Downtown were harmonised to this temporal resolution. *This averaging period was considered appropriate to focus on PM_{10} sources influencing the urban background on representative temporal and spatial scales, while also ensuring robust statistics over the multi-year dataset analysed in this study. Nevertheless, the RASPBERRY algorithm can in principle be applied to data at higher temporal resolution when appropriate measurements and signal-to-noise conditions are available.*

RC8. L290-291: "no thorough assessment exists for the measurement uncertainties or detection limits associated with the optical spectrometer used in this work." – There have been other studies on uncertainties associated with optical-based particle sizing instrument (e.g., UHSAS by DMT with uncertainties estimated by Kupc et al., AMT, 2018). Have the authors tried Monte Carlo simulation to estimate the particle size and counting statistics uncertainty?

AR8. We thank the reviewer for raising the issue and highlighting relevant literature. It should be noted that the instrument mentioned by the reviewer (UHSAS, DMT) operates primarily in the submicron size range and may not be fully representative of the measurement principles and performance of the Fidas Palas used here, which extends to larger particle diameters.

Anyway, based on this comment, we expanded Sect. S2 with a first-order (seminal) discussion on the OPC measurement uncertainty, which is reported here below.

S2.1 Fidas Palas 200 measurement uncertainty

A comprehensive and instrument-specific assessment of the measurement uncertainty of the optical particle counter (OPC) employed here is beyond the scope of the present work, and full laboratory characterisation of the Fidas system was not feasible within this study. Additionally, such an assessment is inherently challenging for this instrument, as the detected signals are processed dynamically by proprietary algorithms in which particle properties are treated as variable quantities, and intermediate processing steps are not accessible to the user. From a practical standpoint, this limits the possibility of rigorously

quantifying the 'sizing precision' through controlled experiments using synthetic aerosols. It should also be emphasised that the Fidas retrieval algorithm was originally conceived with the aim not to provide an absolute 'true' particle size distribution (PSD), but rather to derive particulate matter (PM) concentrations equivalent to the reference gravimetric method. In this respect, the instrument has been demonstrated to yield PM values with comparatively low uncertainty.

For these reasons, only a simplified and conceptual discussion is reported here. Several sources of uncertainty can be identified:

- ***Counting statistics**. In the present study, PSD data are measured over a time interval of 1* min *and averaged over 1* h. *The effective analysed air volume during 1* h *(i.e. the volume illuminated by the optical beam and effectively probed, which differs from the total flow rate) is approximately* $V_{\mathrm{eff}} \sim 9.2 \times 10^3$ cm^3 *(S. Hogekamp, Palas GmbH, personal communication). An estimate of the number of particles detected in each size bin can be obtained by multiplying the median particle number size distribution reported by the instrument by* V_{eff} *and by* $\log_{10}(D_p)$. *This yields particle counts ranging from approximately* 10^5 *for the smallest diameter bins (*$D_p \sim 0.18$ μm*) to about* 10 *particles at* $D_p \sim 10$ μm. *Assuming Poisson counting statistics, the corresponding relative uncertainty is given by*

$$\frac{\sigma_N}{N} = \frac{1}{\sqrt{N}}, \tag{1}$$

  leading to values in the range 0.16 % to 30 %. It should be considered that ambient PM_{10} *concentrations in Aosta are generally low, and notably large particles are relatively rare. Hence, median conditions as those selected above are not the most relevant circumstances for the application of the RASPBERRY methodology. Considering higher percentiles of the particle number distribution (e.g. 80th–90th percentile) instead of the median leads to increased particle counts and therefore reduced relative uncertainties, of the order of 0.1 % for the smallest particles and 15 % for the largest ones. Notably, the latter is of the same order of magnitude as the uncertainty adopted in the PMF analysis (Sect. S7).*

  It is important to stress that this source of uncertainty arises purely from counting statistics and is therefore common to all particle-counting instruments. In the present estimate, the only instrument-specific parameter is the effective probed volume.

- ***Sensor and sizing uncertainty**. Without going into further detail, it is reasonable to assume that the repeatability of particle sizing for identical, monodisperse particles is on the order of a few percent for the instrument considered here (S. Hogekamp, Palas GmbH, personal communication). This contribution reflects the intrinsic variability of the optical detection and sizing process.*

- ***Multi-channel and modal analysis**. The identification and quantification of PMF factors in the particle size distribution and their PM contributions, as performed in this work, relies on measurements across multiple adjacent size channels. This inherently reduces the impact of the random component of the uncertainty associated with individual bins. The EVLS method employed here (Sect. S9) explicitly propagates both measurement uncertainty and profile uncertainty into the estimation of factor contribution uncertainties, thereby accounting for these effects in a consistent manner.*

Finally, it should be emphasised that the uncertainty values used as input to the PMF analysis are not limited to measurement uncertainties alone. Rather, they are derived through a broader procedure that also accounts for the coexistence of different physical quantities within the source apportionment framework, as well as model-related considerations (Sect. S7).

RC9. L306-307: "Achieving an optimal solution required us several tests, as small variations in the uncertainty configuration often produced unpredictable changes in the final outcome." – Does this

mean that the reported equations for the uncertainty configuration (Eq 4-5) are based on this tuning process?

AR9. We thank the reviewer for raising the point of the limited level of detail originally provided to describe the uncertainty configuration in our approach. Indeed, RASPBERRY reproductivity is actually a goal of this work. To address this potential shortcoming, while at the same time keeping the main text concise, we expanded Sect. S7 of the Supplement. In particular, we now provide a complete description of the procedure used to determine the optimal uncertainty configuration. This workflow is presented in an objective and reproducible manner. We also removed the term 'heuristic', which – although commonly used in the PMF literature – may give the misleading impression that the parameter selection was excessively subjective or arbitrary.

The revised text reads:

The uncertainty framework employed in this study follows the methodology outlined by Vörösmarty et al. (2024), in which the PMF input uncertainty is parametrised as in Eqs. (4) and (5) of the main text. This formulation essentially represents a semi-empirical error model, with notation likely inherited from earlier PMF implementations (PMF2), and separates the uncertainty into two components representing common sources of uncertainty in aerosol measurements: (i) baseline instrument/analysis noise, ensuring a minimum uncertainty even when concentrations are small; and (ii) a concentration-dependent error, which increases proportionally with the measured concentration. The interested reader is referred to that work, and the references therein, for further details. Here we instead present an objective and reproducible workflow describing, step by step, how the free coefficients A, α, and C_3 were selected:

1. *Choice for A and α started from relevant ranges suggested in the aforementioned study and in the scientific literature (e.g., Zhou et al., 2005a; Ogulei et al., 2006, 2007; Gu et al., 2011), i.e. 0.01 to 0.05 for the product $A \times \alpha$. In our case, $A = 1$ was assigned to size channels and optical absorption, and $\alpha = 0.01$ was used as an initial value, following Vörösmarty et al. (2024).*

2. *Choice for C_3 started from values between 0.01 and 0.5. For example, Vörösmarty et al. (2024) select 0.10 for most of their channels. A value of 10 % represents a reasonable a priori estimate of the uncertainty when no additional information is available, therefore C_3 was initially set to this value in our case.*

3. *We then ensured that the total variable (e.g., PM_{10}) did not influence the factorisation by setting it as 'weak' in the PMF (or by assigning $A = 3$ and $C_3' = C_3 \times 3$).*

4. *An initial PMF run was performed, and the residual distribution (Q/Q_{exp}) for each 'species' (VSD channels from OPC and aethalometer spectral absorption at the measured wavelengths) was recorded. At this stage, the volume distribution component typically dominated the profile splitting and was better reproduced by the PMF, with the exception of the largest size ranges (as also reported by Vörösmarty et al., 2024), whereas spectral absorption contributed only marginally to the separation and was not well reproduced (resulting in a high Q/Q_{exp} ratio). This behaviour arises from the larger number of 'channels' associated with particle size (OPC measurements) compared with those related to multispectral optical absorption (aethalometer). This imbalance was corrected in the subsequent steps.*

5. *We gradually adjusted the uncertainty until three criteria were simultaneously satisfied: (i) the factor contributions remained as uncorrelated as possible; (ii) the scaled residuals fell within the expected range (± 3, Norris et al., 2014); and (iii) the resulting profiles and contributions were physically plausible.*

6. *In our case, reducing the residuals (and the Q/Q_{exp} ratio) for the largest size channels without artificially splitting the coarse 'local resuspension' factor into two modes required increasing their uncertainty. This resulted in $C_3 = 0.3$ for size channels with particles larger than $2\,\mu m$ and $C_3 = 0.4$ for particles above $6\,\mu m$. The $2\,\mu m$ and $6\,\mu m$ thresholds were selected as representative of the desert*

dust and coarse resuspension modes, based on previous literature (see main text) and the examination of the temporal evolution of the volume size distributions. Indeed, these C_3 values improved the separation between desert dust and local resuspension contributions. Larger uncertainty values tended to merge these contributions, whereas smaller values tended to split the local resuspension factor into multiple modes.

7. *Conversely, in order for the absorption measurements to contribute effectively to shaping the factor profiles, their uncertainty had to be reduced. In this study, C_3 was set to 0.05 for aethalometer measurements. Using higher values caused the size-related portion of the PMF to dominate due to the larger number of size classes, leading to additional size modes lacking clear physical interpretation. In some configurations, the contributions associated with traffic emissions and residential biomass burning became unrealistically small. Similar issues concerning the mass of the traffic factor were reported by Forello et al. (2023). Notably, the selected configuration yielded PM_{10} contributions for traffic and biomass burning that are consistent with the method described by Aujay-Plouzeau (2020), which is based solely on aethalometer measurements.*

8. *During this process, it was necessary to increase the number of factors relative to the initial run, which was based only on size, in order to accommodate factors emerging from the multispectral absorption-driven splitting (e.g., traffic, biomass burning, condensation-mode secondary aerosols). More details on the selection of the optimal number of factors are provided in Sect. S11.*

9. *The plot of the original and reconstructed time series were examined for each input species to verify whether the selected uncertainty configuration reproduced the original data satisfactorily.*

10. *Note that α primarily affects the PMF behaviour at low concentrations of a species, whereas C_3 influences the behaviour at medium to high concentrations. This distinction is particularly important for species exhibiting a marked seasonal cycle, such as those related to biomass burning. In such cases, the minimum uncertainty (constant component, see Table S1) should be chosen so that winter and summer conditions are clearly distinguished, i.e. situations in which the species is present or absent in the atmosphere are well separated.*

11. *The factor uncertainties were finely adjusted at the end of the procedure by scaling them so that the residuals fell within the expected range of ± 3. In this study, an additional 20 % increase in all C_3 values was required. The coefficients were scaled accordingly rather than introducing an additional parameter ('Additional model uncertainty') in EPA PMF 5.0. The C_3 values reported in Table S1 include this factor and their reported digits are approximated to ± 0.05 for clarity.*

The final values for the parameters A, α, and C_3 are shown in Table S1. [...]

It may be noted that:

- *The uncertainty assigned to the largest size channels ($d > 6\,\mu m$) is relatively high. This reflects the low number concentration of large particles and their 'shot' nature, which introduces greater variability when considered from a Poisson-based perspective (Sect. S2.1). Indeed, these bins typically contain a few peak values emerging from a background of zeros, whose frequency can reach up to 30 %. Consequently, these size channels, together with the total variable PM_{10}, were classified as weak variables in the PMF configuration to prevent them from exerting excessive influence during subsequent tests. During the testing phase, as suggested in previous studies (e.g., Zhou et al., 2004; Thimmaiah et al., 2009; Zhou et al., 2005b), an alternative approach was also evaluated in which the largest size bins were grouped (in sets of three to five, depending on particle size) to mitigate issues associated with low particle counts and to improve the signal-to-noise ratio (SNR). Although bin grouping effectively increased the SNR, it hindered the separation of the two coarse factors (desert dust and local resuspension). For this reason, this approach was not adopted in the final configuration.*

- *The NeBC uncertainties used in this study are lower than those reported in some previous works (e.g., Forello et al., 2019; Rigler et al., 2020). In particular, Forello et al. (2023) applied an uncertainty as high as 50 % for b_{abs} to avoid convergence issues when coupling absorption data with chemical data*

in the PMF. With such high uncertainty values, combined with the smaller number of optical variables relative to chemical species, the NeBC information effectively follows the factorisation rather than contributing to it. In contrast, the present approach aims to ensure that both spectral absorption and volume size distribution contribute to determining the final solution. Consequently, the uncertainty values adopted here should not be interpreted as strict measurement uncertainties, but rather as weighting parameters used to balance the influence of the different input variables on the Q metric.

RC10. L329-330: For the random subset of 4000 samples, the authors picked samples for all seasons. Did the authors also include data representative of diurnal or temporal trend?

AR10. We agree that this detail was not explicitly stated in the original manuscript. This information has now been added to the revised manuscript, Sect. 3.2: *Owing to the continuous 24 h measurement coverage in the original dataset, the random sampling procedure also results in a nearly homogeneous distribution of observations throughout the day. For example, when considering four day-quarter intervals (0–6, 6–12, 12–18, and 18–24 h), the maximum deviation from a uniform distribution is approximately 3 %.*

This is illustrated in Fig. 1 in this document for the reviewer's reference.

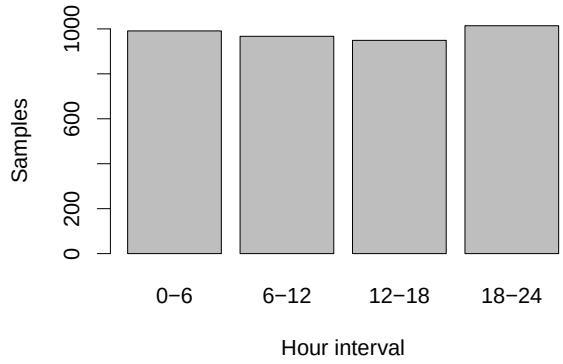

Figure 1: Frequency distribution of samples used for RASPBERRY training across day quarters.

The random subset is also considered representative of the temporal trend.

RC11. L340: "assuming the profiles remain stable over time". If the profiles are different, how does RASPBERRY handle this? Would it generate inaccurate source apportionment?

AR11. Yes, this is indeed a potential limitation, and it is not specific to RASPBERRY but applies to any source apportionment technique relying on fixed source profiles.

Based on the reviewer's comment, the main text has been updated and Sect. 5 (Discussion) now reads:

Another limitation of using fixed source profiles is unsuitability for assessing long-term trends. Genuine changes in emission sources over time, such as variations in vehicle fleets, fuel types, or residential heating practices, as well as instrumental drifts could affect the measured size distribution and light absorption properties of aerosols (e.g., Grange et al., 2020), potentially leading to less accurate retrievals. More advanced approaches exist that allow a certain degree of flexibility in the profiles (e.g. the multilinear engine implemented in SoFi), but the objective of the present study was to introduce a simple and easily reproducible methodology. In practice, the impact of potential profile variability can be assessed a posteriori using regression-based diagnostics to evaluate the quality of the fit. These metrics allow the identification of situations in which the prescribed profiles are not fully (or no more) representative of the observations. Instrumental sensitivity changes must also be carefully monitored and corrected, ideally through regular comparisons with alternative techniques (e.g., EC measurements using the thermo-optical transmission method against NeBC from the aethalometer). In our case, no systematic degradation of the fit quality was observed as a function of season or over the 5-year study period, suggesting that the assumption of stable profiles is reasonable for the dataset analysed here.

RC12. Figure 3: I would plot particle diameters (right column) on a log scale instead of a linear scale.

AR12. The particle diameter (x) axis in the right-hand column was already on a logarithmic scale. The figure caption has been updated to include this information.

RC13. L475: The authors mentioned that residential biomass burning agree with previous studies that detected maxima around 100-200 nm. Since the OPC cannot measure below 180 nm, we cannot actually see any peak below this detection limit. I would not claim this in the manuscript.

AR13. We agree with the reviewer. The sentence has been removed from the manuscript.

RC14. L447: Reported AAEs on Fig. 3 are rounded to 1 decimal point. I would keep that consistency in the manuscript: 1.1 and 1.8 instead of 1.06 and 1.79.

AR14. The AAE values reported in the manuscript have now been rounded to one decimal point.

RC15. Figure 7 caption: There is no 'pink' color in panel (a). Did the authors mean 'yellow'?

AR15. Thank you, the colour description has now been changed to 'yellow'.

RC16. L626: The elevated baseline of RASPBERRY vs. CAMS ensemble – is this indicative of CAMS ensemble not capturing the background desert dust level OR is it an issue with RASPBERRY algorithm?

The authors should add some explanation for this discrepancy between the 2 datasets.

AR16. The elevated baseline of RASPBERRY compared to the CAMS ensemble may indeed reflect a combination of factors, rather than a single cause.

To further investigate this aspect, we analysed the baseline by removing the main dust peaks and excluding data within ±12 h of such events. The resulting mean baseline contribution is approximately 2 $\mu g, m^{-3}$, which is likely compatible with the overall uncertainty associated with PM measurements and source apportionment. Interestingly, this 'background-only' time series exhibits a pronounced diurnal cycle (with a morning maximum), a clear weekly pattern (including a weekend effect), a main peak in July, and a secondary maximum in October.

These features suggest that the baseline identified by RASPBERRY is not purely an artefact, but may instead reflect real processes that are not fully captured by the CAMS ensemble. In particular, it is plausible that this contribution is associated with the resuspension of relatively fine crustal particles (of either desert or local origin), driven by traffic and modulated by road surface moisture. Such processes are known to produce temporally structured signals that may not be adequately represented in large-scale models.

These considerations are consistent with the broader interpretation already provided in the main text (lines 657–661 in the previously submitted manuscript), which was partly updated as follows:

The overall average contributions of these two factors to the total PM_{10} in the period 2020–2024 are 3.6 $\mu g m^{-3}$ (21 %) for desert dust and 3.7 $\mu g m^{-3}$ (21 %) for local resuspension of coarser particles, together accounting for more than 40 % of the total PM_{10}. Such a large percentage contribution is justified by the substantial volume carried by these coarse particles and the relatively low contributions from other local sources at this lightly polluted measurement site. In particular, according to RASPBERRY desert dust estimates, 22 out of the 36 PM_{10} daily exceedances recorded in Aosta–Downtown during the five-year study period (as defined by the new 2024 AAQD; 16 out of the 26 under the current 2008 AAQD) could in fact be excluded from the count due to the contribution of natural sources. *At the same time, we acknowledge that a slight overestimation of the desert dust contribution by RASPBERRY may be possible. Indeed, after removing peak events and data within* ±12 *hours of such episodes, the residual baseline averages* ~ 2 $\mu g m^{-3}$*, a value compatible with PM measurement uncertainty. Notably, this baseline exhibits a distinct diurnal and weekly variability (including a morning maximum and weekend effect), as well as seasonal features (peaks in July and October), suggesting a contribution from the resuspension of fine crustal particles (of desert or local origin) driven by traffic and modulated by road surface moisture.* Despite these limitations, factor 5 remains highly effective for identifying desert dust events and the overall results remain qualitatively consistent with similar dynamics observed in other southern European regions.

RC17. Figure 8 right column: It would account for uncertainties in both chemical PMF and RASPBERRY algorithm if the authors apply ODR fitting instead of OLS. It would change the slope value drastically depending on what the uncertainty estimates may be.

AR17. Based on this very relevant comment, the manuscript was significantly expanded. First, as already reported in our Author Response #2, the effective variance least squares method was introduced to propagate the measurement and profile uncertainties into each RASPBERRY retrieval. Second, new figures and tables, reported here below, have been introduced in the Supplement, including York et al. (2004) regression, which we verified to produce coefficients identical to those obtained using ODR.

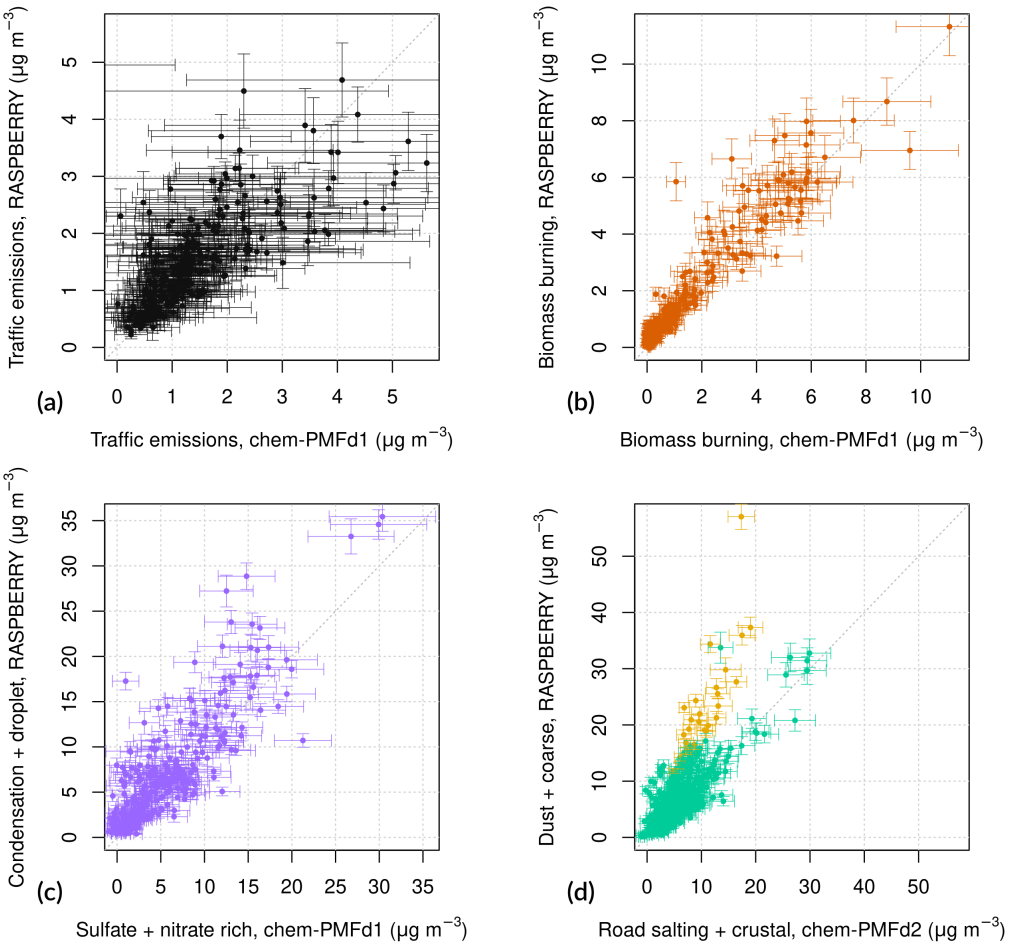

Figure 2: **[Now Figure S34 in the revised supplement]** Comparison of daily-averaged PM_{10} source contributions derived from the chemical PMFs (further reprocessed using EVLS) and RASPBERRY+EVLS, shown together with their individual uncertainties. The plots include only samples from coincident dates in both datasets, limiting the comparison to the subperiod 2020–2021. Subfigure **(c)** represents the comparison between the sum of the sulfate- and nitrate-rich factors from the chemical PMF and the sum of the condensation- and droplet-mode factors from RASPBERRY+EVLS. Subfigure **(d)** illustrates the comparison between the sum of the road-salting and crustal factors from the chemical PMF (dataset 2) and the sum of desert dust and local dust resuspension from RASPBERRY+EVLS. Data influenced by significant Saharan dust events are shown in yellow in subfigure **(d)**.

Table 1: Regression coefficients and their standard errors between the PM_{10} contributions from the chemical PMF (x) and RASPBERRY(+EVLS) (y), determined using different regression methods: ordinary least squares (OLS), Deming regression (total least squares, Linnet, 1990), York regression (York et al., 2004), and log-log York regression to account for heteroscedasticity.

Method	Coefficients	Traffic	Biomass burning	Secondary [a]	Coarse [b]
OLS	Slope	0.58 ± 0.04	0.99 ± 0.02	0.99 ± 0.04	0.95 ± 0.03
	Intercept ($\mu g m^{-3}$)	0.72 ± 0.06	0.34 ± 0.04	1.62 ± 0.28	1.36 ± 0.19
Deming [c]	Slope	0.60 ± 0.05	1.08 ± 0.04	1.08 ± 0.05	0.96 ± 0.05
	Intercept ($\mu g m^{-3}$)	0.70 ± 0.09	0.22 ± 0.03	1.16 ± 0.24	1.31 ± 0.20
York [d]	Slope	1.35 ± 0.12	1.20 ± 0.03	1.32 ± 0.03	1.58 ± 0.03
	Intercept ($\mu g m^{-3}$)	-0.16 ± 0.11	0.12 ± 0.01	0.01 ± 0.12	-0.88 ± 0.08
York (log)	Slope	1.05 ± 0.08	0.86 ± 0.02	1.26 ± 0.04	1.32 ± 0.02
	Intercept ($\mu g m^{-3}$)	0.01 ± 0.05	0.32 ± 0.02	-0.51 ± 0.08	-0.41 ± 0.03

[a] Sum of sulfate- and nitrate-rich factors from the chemical PMF, and condensation and droplet mode factors from RASPBERRY.
[b] Sum of road salting and crustal factors from the chemical PMF, and desert dust and local dust resuspension from RASPBERRY, excluding data influenced by significant Saharan dust events.
[c] The regression was performed taking into account the actual variance-error ratios obtained from the DISP test of both physical and chemical PMFs. RASPBERRY retrievals were used with this method.
[d] The regression was performed using individual uncertainties calculated through EVLS for both the physical (RASPBERRY+EVLS) and chemical (PMF+EVLS) data sets (Fig. S34). York et al. (2004) regression yields the same coefficients as those obtained using Python's implementation of orthogonal distance regression (ODR).

The main text (Sect. 4.3) was updated accordingly:

To evaluate the comparison, we use the coefficients of the regression equation relating the source contributions from the physical source apportionment (y) to those from the chemical PMF (x), together with the corresponding explained variance (R^2). For the sake of simplicity, we report in the main text only the coefficients obtained using traditional ordinary least squares (OLS) regression. The interested reader can find the results obtained with alternative, more advanced regression approaches in Table S3 and Fig. S34, namely: (i) total least squares (Deming regression; Linnet, 1990), performed by accounting for the actual variance-error ratios obtained from the DISP test of both the physical and chemical PMF solutions; (ii) York regression (York et al., 2004), performed using individual uncertainties calculated through EVLS for both the physical (RASPBERRY+EVLS) and chemical (PMF+EVLS) data sets; and (iii) York regression applied to log-transformed quantities to account for heteroscedasticity in the data.

The comparison of traffic factors is depicted [...] This deviation can be attributed to difficulties in accurately identifying the traffic factor, primarily due to the following reasons: [...] Contributions from both source apportionments are relatively low, steadily remaining below 6 $\mu g m^{-3}$, which is consistent with the fact that Aosta is a relatively small, low-traffic city (33,000 inhabitants; Diémoz et al., 2019, 2020, 2021). At the same time, the relative uncertainty associated with traffic emissions is among the highest of all dimensional profiles. This is evident from both the large interval ratio obtained from the DISP test (Sect. 4.2 and Fig. 3) and from the uncertainties derived using the EVLS method for both the physical and the chemical data sets (Fig. S34) [...]

At the same time, it should be noted that the comparison slope for the traffic factor is higher than 1 when using York and log-transformed York regressions (Table S3), since the intercept decreases. Therefore, the deviation from the 1:1 line may also be partly attributable to an artefact of the regression method itself.

For the secondary particles [...] the large positive intercept is statistically significant when using OLS and Deming regressions, but not with York regression, and it turns negative (and statistically significant) when York regression is applied to log-transformed data. This result suggests that, similarly to traffic, the apparent high bias is largely an artefact of the regression method, and perhaps of the heteroscedastic nature of the data, rather than a systematic discrepancy between the two source apportionment approaches.

RC18. Figure 13: The color of the maximum values for both AOD and CO color bars are too similar, so I suggest the authors to change colors on one of the color bars.

AR18. The colour scales have been revised and the updated maps are presented in Fig. 3 of the present document. In addition, carbon monoxide concentrations at 500 hPa derived from AIRS/Aqua have been updated to v6 STD, Level 3, providing an improved representation.

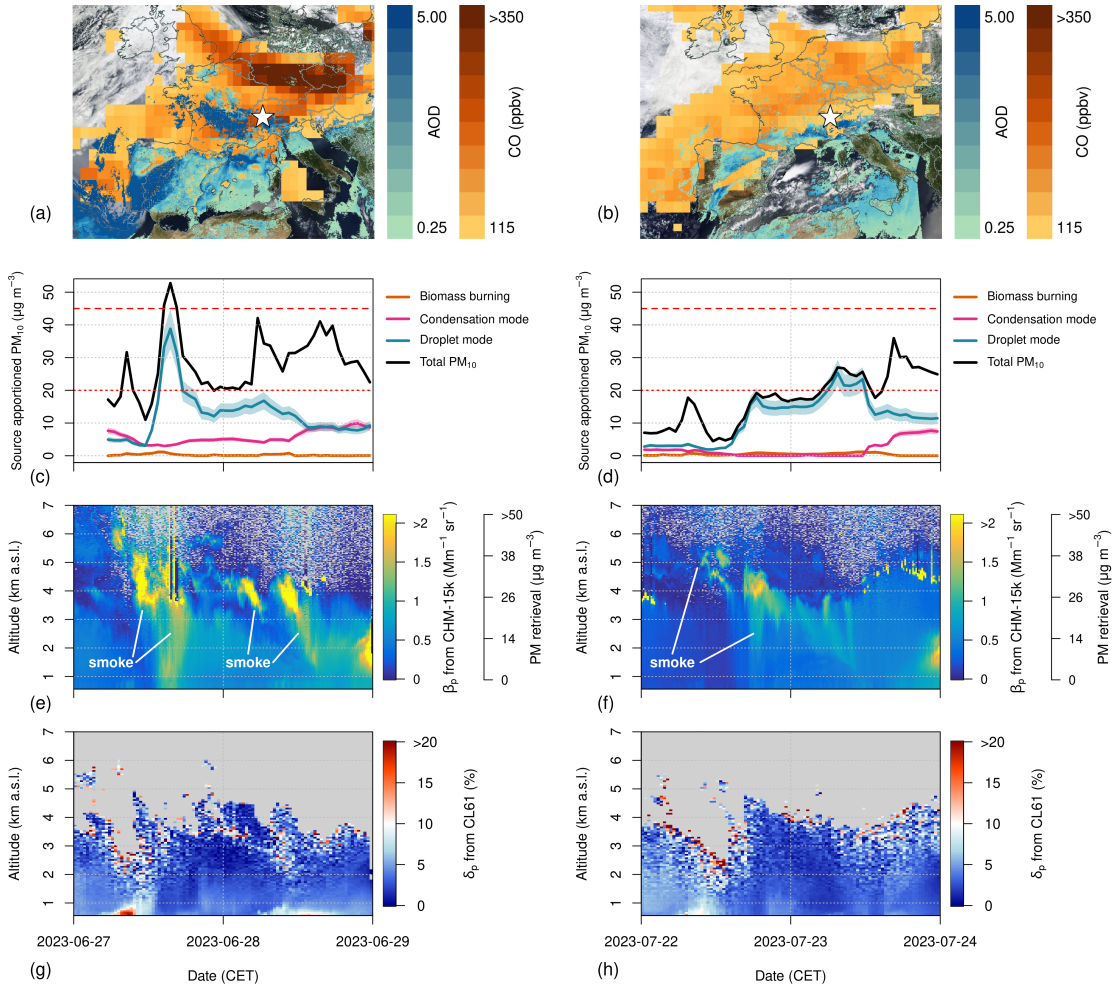

Figure 3: Transport of smoke from Canada to Europe in summer 2023. **(a, b)** Satellite images (27 June and 22 July 2023) with background from MODIS/Terra corrected reflectance. Aosta is indicated by a star marker. Aerosol Optical Depth (AOD) at 470 nm, retrieved from the MODIS spectroradiometer onboard the Terra and Aqua satellites (MAIAC algorithm, v6.1 STD, 1-km resolution), and carbon monoxide concentrations at 500 hPa from daytime AIRS/Aqua measurements (v6 STD, L3) are superimposed using two different colour scales (source: `worldview.earthdata.nasa.gov`). **(c, d)** PM_{10} contributions from the condensation and droplet modes, derived from RASPBERRY. Red horizontal lines: PM_{10} limit values introduced by the 2024/2881/EC AQ directive plotted as reference. **(e, f)** Vertical profiles of ALICENET PM retrievals, based on CHM-15k ALC particle backscatter measurements. **(g, h)** Particle depolarisation ratio from the CL61 ALC. Note that, in this case, the low smoke depolarisation, together with the weak signal-to-noise ratio of the CL61, limits reliable depolarisation measurements to the lowest atmospheric layers.

RC19. L918-923 paragraph: Have the authors considered comparing the constraining profiles from Po Valley against those collected during the AEROMMA 2023 field mission over North America? The relatively complete aerosol in-situ measurements (3 nm to ~50 um) would provide additional examples of constraining profiles. There were sampling in a lot of megacities (NY, Toronto, Chicago, LA) that captured biomass-burning-influenced aerosols from Canadian wildfires as well as urban pollutions. Despite the geographic differences, I highly suggest the authors to compare the aerosols profiles to provide additional constraining profiles for RASPBERRY.

AR19. Thank you very much for raising this important point. Indeed, the availability of a priori 'constraining' particle number size distribution (PNSD) profiles measured at the surface and already apportioned to individual sources would enable the direct implementation of the CMB-like RASPBERRY approach (i.e. the 'retrieval phase'), potentially bypassing the 'training phase' based on PMF. However, this would require source-specific profiles that are highly representative of the conditions at the sampling site under investigation. Unfortunately, existing literature indicates that source-related PNSD profiles exhibit significant variability as a function of location and sampling period (e.g. interannual variability), reflecting changes in source characteristics and atmospheric processing (Kim et al., 2004; Gu et al., 2011; Vu et al., 2015; Leoni et al., 2018; Rivas et al., 2020; Hopke et al., 2022; Harni et al., 2024). In light of the reviewer's suggestion, we have nevertheless examined the available literature reporting in-situ surface measurements of source-resolved PNSDs and PVSDs, including datasets from recent intensive field campaigns where available, in order to compare them with those derived from RASPBERRY and presented in Fig. 3 of the main text. This literature review has now been incorporated into Sect. S14 of the Supplement and is summarised below.

1. ***Traffic:*** *As stated in the manuscript, the PVSD exhibits a multimodal structure, indicating contributions from composite sources (Mazzei et al., 2007; Cuccia et al., 2010). A maximum is observed at the lower limit of the diameter range (180* nm*), suggesting potentially higher VSD values for smaller particles associated with traffic exhaust (Costabile et al., 2009; El Haddad et al., 2009; Gu et al., 2011; Dall'Osto et al., 2012; Wu et al., 2021), followed by a second mode attributable to resuspension processes. Indeed, Gu et al. (2011), Liu et al. (2014), and Leoni et al. (2018) reported a first PVSD maximum at ~100–200* nm *and a second one at ~4–5* μm*. The latter is consistent with our local PVSD maximum (3.53* μm*) above 1* μm*, indicating the contribution of non-exhaust emissions. Considering 'fresh traffic' emissions, these can only be approximated by log-normal interpolation of our OPC data (e.g., Ferrero et al., 2011, 2014, 2019). Acknowledging the limitations of such an approach when applied to raw OPC data, the estimated volume mean diameter (VMD) of this factor in RASPBERRY is ~100* nm*, corresponding to a count mean diameter (CMD) of ~50* nm *and a geometric standard deviation (GSD) of 1.61. These values are consistent with the aforementioned studies and support the interpretation of Factor 1.*

2. ***Residential biomass burning:*** *The PVSD exhibits a maximum at 305* nm *and shows an increasing trend towards the lower limit of the diameter range (180* nm*). Gu et al. (2011), Liu et al. (2014), and Leoni et al. (2018) reported PVSD maxima in the ~100–500* nm *range, with CMD values between 40 and 170* nm*. Applying log-normal interpolation to our OPC data yields an estimated VMD of ~230* nm*, corresponding to a CMD of ~170* nm *with a GSD of 1.37. These values lie towards the upper end of the reported ranges, however the presence of a local minimum at 264* nm *(Fig. 3d) partially affects the log-normal fitting.*

3. ***Secondary aerosol (condensation mode):*** *The aforementioned studies by Gu et al. (2011), Liu et al. (2014), and Leoni et al. (2018) reported PVSD peaks at approximately ~500, ~250, and ~300* nm*, respectively. The RASPBERRY PVSD associated with this factor is relatively smooth, with an OPC maximum at 264* nm*. Log-normal interpolation of the OPC data provides an estimated VMD of ~240* nm*, corresponding to a CMD of ~220* nm *and a GSD of 1.18, in good agreement with previous studies.*

4. ***Secondary aerosol (droplet mode):*** *RASPBERRY PVSD exhibits a bimodal structure below 1* μm*. The second peak is close to the 'accumulation mode' at ~400* nm *reported by Liu et al. (2014), the 'secondary aerosol' at ~500* nm *described by Gu et al. (2011), and differs from the 'regional pollution'*

mode at ~900 nm *reported by Leoni et al. (2018). The first peak (~305* nm*) is comparable to the 'aged traffic' mode in Gu et al. (2011) (~200* nm*), the 'secondary ammonium nitrate and sulphate' mode in Liu et al. (2014) (~250* nm*), and the 'urban background' mode in Leoni et al. (2018) (~250* nm*). Overall, this droplet mode appears to represent a complex mixture of urban and regional background aerosols. Log-normal interpolation yields a first VMD of ~310* nm *(CMD ~270* nm*, GSD 1.23) and a second VMD of ~500* nm *(CMD ~440* nm*, GSD 1.22), in good agreement with previous findings.*

5. ***Desert dust:*** *RASPBERRY PVSD peaks at 4.072* μm*. Log-normal interpolation yields a VMD of ~3.94* μm*, corresponding to a CMD of ~2.50* μm *with a GSD of 1.48. The dust peak reported by Liu et al. (2014) ('fugitive dust', not directly comparable) lies above 1* μm*, although the upper size limit prevents identification of the maximum. Gu et al. (2011) reported a peak at ~3* μm*, which is consistent with our findings. It is noted that Leoni et al. (2018) did not identify a desert dust factor.*

6. ***Local dust resuspension:*** *RASPBERRY PVSD peaks at 7.782* μm*. Log-normal interpolation yields a VMD of ~5.62* μm*, corresponding to a CMD of ~4.40* μm *with a GSD of 1.33. A comparable resuspension peak is not reported by Liu et al. (2014), whereas Gu et al. (2011) identified two volume peaks at ~300* nm *and ~7* μm*, the latter being consistent with our observations. Similarly, the ~5* μm *peak reported by Leoni et al. (2018) for 'industrial coarse particles/road dust' is in agreement with our results.*

Based on the above comparison, the robustness of our results is further supported. At the same time, the observed differences highlight the variability of size distribution profiles as a function of location, source characteristics, and sampling period (including interannual variability driven by changes in source features, Kim et al., 2004; Gu et al., 2011; Vu et al., 2015; Leoni et al., 2018; Rivas et al., 2020; Hopke et al., 2022; Harni et al., 2024). This suggests that the profiles presented in Fig. 3 may also serve as a valuable reference for future source apportionment studies and inter-comparisons.

RC20. L939-944 paragraph: The authors could add the recommendation of additional in-situ aerosol measurements with more comprehensive instruments (e.g., extend particle size detection to nucleation mode) to provide additional training datasets for RASPBERRY algorithm.

AR20. The recommendation to extend particle size detection down to the nucleation mode through the inclusion of additional in situ aerosol measurements was already mentioned in the original manuscript (lines 910, 960–965, and 1033–1036). Nevertheless, the paragraph referred to by the reviewer (primarily addressing the limitations of fixed source profiles for long-term trend analysis, see Author Response 11) has been further expanded to explicitly include this point. The revised text now reads: *When PM mass is not the only focus, a complementary approach, as already mentioned above, is to incorporate additional in situ aerosol measurements using more comprehensive instrumentation (e.g. extending particle size detection to the nucleation mode), thereby providing enhanced training datasets for the RASPBERRY algorithm and improving the detection of trends in particle size distributions.*

References

Aujay-Plouzeau, R.: Guide méthodologique pour la mesure du «Black Carbon» par Aethalomètre multi longueur d'onde AE33 dans l'air ambiant (Version 2020), Tech. rep., Ineris, https://www.lcsqa.org/system/files/media/documents/LCSQA2019-Guide_mesure_BlackCarbon_par_AE33_VF03-Approuv%C3%A9CPS15122020.pdf, 2020.

Beddows, D., Brean, J., Rowell, A., Merkel, M., Weinhold, K., Dall'Osto, M., and Harrison, R.: Wide-Positive Matrix Factorisation of particle number size distributions: A new approach accounting

for cyclically changing source profiles, Sci. Total Environ., 998, 180 231, https://doi.org/10.1016/j.scitotenv.2025.180231, 2025.

Brown, S. G., Eberly, S., Paatero, P., and Norris, G. A.: Methods for estimating uncertainty in PMF solutions: Examples with ambient air and water quality data and guidance on reporting PMF results, Sci. Total Environ., 518-519, 626–635, https://doi.org/10.1016/j.scitotenv.2015.01.022, 2015.

Chen, J., Dai, Q., Zhang, X., Tian, Y., Feng, Y., and Hopke, P. K.: PMF Source Contribution Uncertainty Estimation via Effective Variance Least Squares, ACS ES&T Air, 2, 3045–3053, https://doi.org/10.1021/acsestair.5c00312, 2025.

Ćirović, Ž., Stojanović, D. B., Davidović, M., Onjia, A., Alastuey, A., and Jovašević-Stojanović, M.: New Particle Formation and Source Apportionment of Particle Number Size Distribution in the Urban Area of the City of Belgrade, Atmosphere, 17, https://doi.org/10.3390/atmos17020205, 2026.

Costabile, F., Birmili, W., Klose, S., Tuch, T., Wehner, B., Wiedensohler, A., Franck, U., König, K., and Sonntag, A.: Spatio-temporal variability and principal components of the particle number size distribution in an urban atmosphere, Atmos. Chem. Phys., 9, 3163–3195, https://doi.org/10.5194/acp-9-3163-2009, 2009.

Coulter, C. T.: EPA-CMB8. 2 users manual, US. Environmental Protection Agency, Office of Air Quality Planning & Standards, Emissions, Monitoring & Analysis Division, Air Quality Modeling Group, https://www.epa.gov/sites/default/files/2020-10/documents/epa-cmb82manual.pdf, 2004.

Cuccia, E., Bernardoni, V., Massabò, D., Prati, P., Valli, G., and Vecchi, R.: An alternative way to determine the size distribution of airborne particulate matter, Atmos. Environ., 44, 3304–3313, https://doi.org/10.1016/j.atmosenv.2010.05.045, 2010.

Dall'Osto, M., Beddows, D. C. S., Pey, J., Rodriguez, S., Alastuey, A., Harrison, R. M., and Querol, X.: Urban aerosol size distributions over the Mediterranean city of Barcelona, NE Spain, Atmos. Chem. Phys., 12, 10 693–10 707, https://doi.org/10.5194/acp-12-10693-2012, 2012.

Diémoz, H., Gobbi, G. P., Magri, T., Pession, G., Pittavino, S., Tombolato, I. K. F., Campanelli, M., and Barnaba, F.: Transport of Po Valley aerosol pollution to the northwestern Alps – Part 2: Long-term impact on air quality, Atmos. Chem. Phys., 19, 10 129–10 160, https://doi.org/10.5194/acp-19-10129-2019, 2019.

Diémoz, H., Tombolato, I. K. F., Zublena, M., Magri, T., and Ferrero, L.: The impact of biomass burning emissions on PM concentration in the Greater Alpine region, in: Proceedings of 12th International Conference on Air Quality, Science and Application, p. 26, Hatfield, UK, 10.18745/pb.22217, 2020.

Diémoz, H., Magri, T., Pession, G., Tarricone, C., Tombolato, I. K. F., Fasano, G., and Zublena, M.: Air Quality in the Italian Northwestern Alps during Year 2020: Assessment of the COVID-19 «Lockdown Effect» from Multi-Technique Observations and Models, Atmosphere, 12, https://doi.org/10.3390/atmos12081006, 2021.

El Haddad, I., Marchand, N., Dron, J., Temime-Roussel, B., Quivet, E., Wortham, H., Jaffrezo, J. L., Baduel, C., Voisin, D., Besombes, J. L., and Gille, G.: Comprehensive primary particulate organic characterization of vehicular exhaust emissions in France, Atmos. Environ., 43, 6190–6198, https://doi.org/10.1016/j.atmosenv.2009.09.001, 2009.

Ferrero, L., Mocnik, G., Ferrini, B., Perrone, M., Sangiorgi, G., and Bolzacchini, E.: Vertical profiles of aerosol absorption coefficient from micro-Aethalometer data and Mie calculation over Milan, Sci. Total Environ., 409, 2824–2837, https://doi.org/10.1016/j.scitotenv.2011.04.022, 2011.

Ferrero, L., Castelli, M., Ferrini, B. S., Moscatelli, M., Perrone, M. G., Sangiorgi, G., D'Angelo, L., Rovelli, G., Moroni, B., Scardazza, F., Močnik, G., Bolzacchini, E., Petitta, M., and Cappelletti, D.: Impact of black carbon aerosol over Italian basin valleys: high-resolution measurements along vertical profiles, radiative forcing and heating rate, Atmos. Chem. Phys., 14, 9641–9664, https://doi.org/10.5194/acp-14-9641-2014, 2014.

Ferrero, L., Ritter, C., Cappelletti, D., Moroni, B., Močnik, G., Mazzola, M., Lupi, A., Becagli, S., Traversi, R., Cataldi, M., Neuber, R., Vitale, V., and Bolzacchini, E.: Aerosol optical properties in the Arctic: The role of aerosol chemistry and dust composition in a closure experiment between Lidar and tethered balloon vertical profiles, Sci. Total Environ., 686, 452–467, https://doi.org/10.1016/j.scitotenv.2019.05.399, 2019.

Forello, A. C., Bernardoni, V., Calzolai, G., Lucarelli, F., Massabò, D., Nava, S., Pileci, R. E., Prati, P., Valentini, S., Valli, G., and Vecchi, R.: Exploiting multi-wavelength aerosol absorption coefficients in a multi-time resolution source apportionment study to retrieve source-dependent absorption parameters, Atmos. Chem. Phys., 19, 11 235–11 252, https://doi.org/10.5194/acp-19-11235-2019, 2019.

Forello, A. C., Cunha-Lopes, I., Almeida, S. M., Alves, C. A., Tchepel, O., Crova, F., and Vecchi, R.: Insights on the combination of off-line and on-line measurement approaches for source apportionment studies, Sci. Total Environ., 900, 165 860, https://doi.org/10.1016/j.scitotenv.2023.165860, 2023.

Grange, S. K., Lötscher, H., Fischer, A., Emmenegger, L., and Hueglin, C.: Evaluation of equivalent black carbon source apportionment using observations from Switzerland between 2008 and 2018, Atmos. Meas. Tech., 13, 1867–1885, https://doi.org/10.5194/amt-13-1867-2020, 2020.

Gu, J., Pitz, M., Schnelle-Kreis, J., Diemer, J., Reller, A., Zimmermann, R., Soentgen, J., Stoelzel, M., Wichmann, H.-E., Peters, A., and Cyrys, J.: Source apportionment of ambient particles: Comparison of positive matrix factorization analysis applied to particle size distribution and chemical composition data, Atmos. Environ., 45, 1849–1857, https://doi.org/10.1016/j.atmosenv.2011.01.009, 2011.

Harni, S. D., Aurela, M., Saarikoski, S., Niemi, J. V., Portin, H., Manninen, H., Leinonen, V., Aalto, P., Hopke, P. K., Petäjä, T., Rönkkö, T., and Timonen, H.: Source apportionment of particle number size distribution at the street canyon and urban background sites, Atmos. Chem. Phys., 24, 12 143–12 160, https://doi.org/10.5194/acp-24-12143-2024, 2024.

Hopke, P. K., Feng, Y., and Dai, Q.: Source apportionment of particle number concentrations: A global review, Sci. Total Environ., 819, 153 104, https://doi.org/10.1016/j.scitotenv.2022.153104, 2022.

Kim, E., Hopke, P. K., Larson, T. V., and Covert, D. S.: Analysis of Ambient Particle Size Distributions Using Unmix and Positive Matrix Factorization, Environ. Sci. Tech., 38, 202–209, https://doi.org/10.1021/es030310s, 2004.

Leoni, C., Pokorná, P., Hovorka, J., Masiol, M., Topinka, J., Zhao, Y., Křůmal, K., Cliff, S., Mikuška, P., and Hopke, P. K.: Source apportionment of aerosol particles at a European air pollution hot spot using particle number size distributions and chemical composition, Environ. Pollut., 234, 145–154, https://doi.org/10.1016/j.envpol.2017.10.097, 2018.

Linnet, K.: Estimation of the linear relationship between the measurements of two methods with proportional errors, Stat. Med., 9, 1463–1473, https://doi.org/10.1002/sim.4780091210, 1990.

Liu, Z., Hu, B., Liu, Q., Sun, Y., and Wang, Y.: Source apportionment of urban fine particle number concentration during summertime in Beijing, Atmos. Environ., 96, 359–369, https://doi.org/10.1016/j.atmosenv.2014.06.055, 2014.

Mapelli, C., Diémoz, H., Contini, D., Dinoi, A., Cesari, D., and Barnaba, F.: Physics-based aerosol source apportionment at the site of Lecce (Italy), Atmos. Res. (under review), 2026.

Masiol, M., Harrison, R. M., Vu, T. V., and Beddows, D. C. S.: Sources of sub-micrometre particles near a major international airport, Atmos. Chem. Phys., 17, 12 379–12 403, https://doi.org/10.5194/acp-17-12379-2017, 2017.

Mazzei, F., Lucarelli, F., Nava, S., Prati, P., Valli, G., and Vecchi, R.: A new methodological approach: The combined use of two-stage streaker samplers and optical particle counters for the characterization of airborne particulate matter, Atmos. Environ., 41, 5525–5535, https://doi.org/10.1016/j.atmosenv.2007.04.012, 2007.

Norris, G., Duvall, R., and Brown, S.: EPA Positive Matrix Factorization (PMF) 5.0 Fundamentals and User Guide, U.S. Environmental Protection Agency Office of Research and Development Washington, DC 20460, https://www.epa.gov/sites/default/files/2015-02/documents/pmf_5.0_user_guide.pdf, ePA/600/R-14/108, 2014.

Ogulei, D., Hopke, P. K., Zhou, L., Pancras, J. P., Nair, N., and Ondov, J. M.: Source apportionment of Baltimore aerosol from combined size distribution and chemical composition data, Atmos. Environ., 40, 396–410, https://doi.org/10.1016/j.atmosenv.2005.11.075, 2006.

Ogulei, D., Hopke, P. K., Chalupa, D. C., , and Utell, M. J.: Modeling Source Contributions to Submicron Particle Number Concentrations Measured in Rochester, New York, Aerosol Sci. Tech., 41, 179–201, https://doi.org/10.1080/02786820601116012, 2007.

Paatero, P., Eberly, S., Brown, S. G., and Norris, G. A.: Methods for estimating uncertainty in factor analytic solutions, Atmos. Meas. Techn., 7, 781–797, https://doi.org/10.5194/amt-7-781-2014, 2014.

Rigler, M., Drinovec, L., Lavrič, G., Vlachou, A., Prévôt, A. S. H., Jaffrezo, J. L., Stavroulas, I., Sciare, J., Burger, J., Kranjc, I., Turšič, J., Hansen, A. D. A., and Močnik, G.: The new instrument using a TC–BC (total carbon–black carbon) method for the online measurement of carbonaceous aerosols, Atmos. Meas. Tech., 13, 4333–4351, https://doi.org/10.5194/amt-13-4333-2020, 2020.

Rivas, I., Beddows, D. C., Amato, F., Green, D. C., Järvi, L., Hueglin, C., Reche, C., Timonen, H., Fuller, G. W., Niemi, J. V., Pérez, N., Aurela, M., Hopke, P. K., Alastuey, A., Kulmala, M., Harrison, R. M., Querol, X., and Kelly, F. J.: Source apportionment of particle number size distribution in urban background and traffic stations in four European cities, Environ. Int., 135, 105 345, https://doi.org/10.1016/j.envint.2019.105345, 2020.

Thimmaiah, D., Hovorka, J., and Hopke, P. K.: Source apportionment of winter submicron prague aerosols from combined particle number size distribution and gaseous composition data, Aerosol Air Qual. Res., 9, 209–236, https://doi.org/10.4209/aaqr.2008.11.0055, 2009.

Vörösmarty, M., Hopke, P. K., and Salma, I.: Attribution of aerosol particle number size distributions to main sources using an 11-year urban dataset, Atmos. Chem. Phys., 24, 5695–5712, https://doi.org/10.5194/acp-24-5695-2024, 2024.

Vu, T. V., Delgado-Saborit, J. M., and Harrison, R. M.: Review: Particle number size distributions from seven major sources and implications for source apportionment studies, Atmos. Environ., 122, 114–132, https://doi.org/10.1016/j.atmosenv.2015.09.027, 2015.

Watson, J. G., Cooper, J. A., and Huntzicker, J. J.: The effective variance weighting for least squares calculations applied to the mass balance receptor model, Atmos. Environ. (1967), 18, 1347–1355, https://doi.org/10.1016/0004-6981(84)90043-X, 1984.

Wu, H., Li, Z., Jiang, M., Liang, C., Zhang, D., Wu, T., Wang, Y., and Cribb, M.: Contributions of traffic emissions and new particle formation to the ultrafine particle size distribution in the megacity of Beijing, Atmos. Environ., 262, 118 652, https://doi.org/10.1016/j.atmosenv.2021.118652, 2021.

York, D., Evensen, N. M., Martínez, M. L., and De Basabe Delgado, J.: Unified equations for the slope, intercept, and standard errors of the best straight line, Am. J. Phys., 72, 367–375, https://doi.org/10.1119/1.1632486, 2004.

Zhou, L., Hopke, P. K., Paatero, P., Ondov, J. M., Pancras, J., Pekney, N. J., and Davidson, C. I.: Advanced factor analysis for multiple time resolution aerosol composition data, Atmos. Environ., 38, 4909–4920, https://doi.org/10.1016/j.atmosenv.2004.05.040, 2004.

Zhou, L., Hopke, P. K., Stanier, C. O., Pandis, S. N., Ondov, J. M., and Pancras, J. P.: Investigation of the relationship between chemical composition and size distribution of airborne particles by partial least squares and positive matrix factorization, J. Geophys. Res., 110, https://doi.org/10.1029/2004JD005050, 2005a.

Zhou, L., Kim, E., Hopke, P. K., Stanier, C., and Pandis, S. N.: Mining airborne particulate size distribution data by positive matrix factorization, J. Geophys. Res., 110, https://doi.org/10.1029/2004JD004707, 2005b.

Response to Referee #3

We thank the reviewer for his/her time and consideration, and for the constructive comments. We are confident that all remarks have been carefully addressed and that the manuscript has been improved accordingly. Our point-by-point response is provided below (text in italics denotes excerpts from the revised manuscript).

Referee's comment 1. This study presents RASPBERRY (Real-time Aerosol Source apportionment using Physics-Based Experimental data and multivaRiate factoR analYsis), a novel PM10 source apportionment framework that integrates particle size distributions and spectrally resolved light absorption into a unified Physical PMF (Positive Matrix Factorization). Applied to a five-year hourly dataset (2020–2024) from an urban background site in the Italian Alps, the method successfully identifies six aerosol source factors and demonstrates strong agreement with traditional chemical source apportionment techniques, ground-based remote sensing, and atmospheric modeling tools. RASPBERRY addresses a critical gap in air quality monitoring: the ability to perform high temporal resolution, real-time, continuous, and cost-effective aerosol source apportionment that is based on measurements of aerosol physical properties. The paper is well written and methodologically sound. The 5-year dataset provides excellent statistical robustness and seasonal coverage. The bootstrapping approach for uncertainty estimation reflects best practices in PMF analysis. Validation with chemical PMF, lidar, AERONET AOD, and CAMS reanalysis are thorough. Overall, this paper represents a meaningful and timely contribution to the aerosol science and air quality communities. There are several minor issues: Comment 1: In line 309, the impact of the selected coefficient A, α, and C_3 are not mentioned. Also it is mentioned that "no other modeling uncertainty was included". But other uncertainty sources are not mentioned here but instead was in discussion. So it should be briefly explained to guide the audience to discussion about the rest of the uncertainties.

Author's response 1. We thank the reviewer for the positive overall assessment and for highlighting the limited level of detail originally provided to describe the impact of the uncertainty parameters. Indeed, RASPBERRY reproductivity is actually a goal of this work. To address this potential shortcoming, while at the same time keeping the main text concise, we expanded Sect. S7 of the Supplement. In particular, we now provide a complete description of the procedure used to determine the optimal uncertainty configuration, including the impact of the selected coefficients A, α, and C_3. This workflow is presented in an objective and reproducible manner.

The revised text reads:

The uncertainty framework employed in this study follows the methodology outlined by Vörösmarty et al. (2024), in which the PMF input uncertainty is parametrised as in Eqs. (4) and (5) of the main text. This formulation essentially represents a semi-empirical error model, with notation likely inherited from earlier PMF implementations (PMF2), and separates the uncertainty into two components representing common

sources of uncertainty in aerosol measurements: (i) baseline instrument/analysis noise, ensuring a minimum uncertainty even when concentrations are small; and (ii) a concentration-dependent error, which increases proportionally with the measured concentration. The interested reader is referred to that work, and the references therein, for further details. Here we instead present an objective and reproducible workflow describing, step by step, how the free coefficients A, α, and C_3 were selected:

1. *Choice for A and α started from relevant ranges suggested in the aforementioned study and in the scientific literature (e.g., Zhou et al., 2005a; Ogulei et al., 2006, 2007; Gu et al., 2011), i.e. 0.01 to 0.05 for the product $A \times \alpha$. In our case, $A = 1$ was assigned to size channels and optical absorption, and $\alpha = 0.01$ was used as an initial value, following Vörösmarty et al. (2024).*

2. *Choice for C_3 started from values between 0.01 and 0.5. For example, Vörösmarty et al. (2024) select 0.10 for most of their channels. A value of 10 % represents a reasonable a priori estimate of the uncertainty when no additional information is available, therefore C_3 was initially set to this value in our case.*

3. *We then ensured that the total variable (e.g., PM_{10}) did not influence the factorisation by setting it as 'weak' in the PMF (or by assigning $A = 3$ and $C_3' = C_3 \times 3$).*

4. *An initial PMF run was performed, and the residual distribution (Q/Q_{exp}) for each 'species' (VSD channels from OPC and aethalometer spectral absorption at the measured wavelengths) was recorded. At this stage, the volume distribution component typically dominated the profile splitting and was better reproduced by the PMF, with the exception of the largest size ranges (as also reported by Vörösmarty et al., 2024), whereas spectral absorption contributed only marginally to the separation and was not well reproduced (resulting in a high Q/Q_{exp} ratio). This behaviour arises from the larger number of 'channels' associated with particle size (OPC measurements) compared with those related to multispectral optical absorption (aethalometer). This imbalance was corrected in the subsequent steps.*

5. *We gradually adjusted the uncertainty until three criteria were simultaneously satisfied: (i) the factor contributions remained as uncorrelated as possible; (ii) the scaled residuals fell within the expected range (± 3, Norris et al., 2014); and (iii) the resulting profiles and contributions were physically plausible.*

6. *In our case, reducing the residuals (and the Q/Q_{exp} ratio) for the largest size channels without artificially splitting the coarse 'local resuspension' factor into two modes required increasing their uncertainty. This resulted in $C_3 = 0.3$ for size channels with particles larger than $2\,\mu m$ and $C_3 = 0.4$ for particles above $6\,\mu m$. The $2\,\mu m$ and $6\,\mu m$ thresholds were selected as representative of the desert dust and coarse resuspension modes, based on previous literature (see main text) and the examination of the temporal evolution of the volume size distributions. Indeed, these C_3 values improved the separation between desert dust and local resuspension contributions. Larger uncertainty values tended to merge these contributions, whereas smaller values tended to split the local resuspension factor into multiple modes.*

7. *Conversely, in order for the absorption measurements to contribute effectively to shaping the factor profiles, their uncertainty had to be reduced. In this study, C_3 was set to 0.05 for aethalometer measurements. Using higher values caused the size-related portion of the PMF to dominate due to the larger number of size classes, leading to additional size modes lacking clear physical interpretation. In some configurations, the contributions associated with traffic emissions and residential biomass burning became unrealistically small. Similar issues concerning the mass of the traffic factor were reported by Forello et al. (2023). Notably, the selected configuration yielded PM_{10} contributions for traffic and biomass burning that are consistent with the method described by Aujay-Plouzeau (2020), which is based solely on aethalometer measurements.*

8. *During this process, it was necessary to increase the number of factors relative to the initial run, which was based only on size, in order to accommodate factors emerging from the multispectral absorption-driven splitting (e.g., traffic, biomass burning, condensation-mode secondary aerosols). More details on the selection of the optimal number of factors are provided in Sect. S11.*

9. *The plot of the original and reconstructed time series were examined for each input species to verify whether the selected uncertainty configuration reproduced the original data satisfactorily.*

10. *Note that α primarily affects the PMF behaviour at low concentrations of a species, whereas C_3 influences the behaviour at medium to high concentrations. This distinction is particularly important for species exhibiting a marked seasonal cycle, such as those related to biomass burning. In such cases, the minimum uncertainty (constant component, see Table S1) should be chosen so that winter and summer conditions are clearly distinguished, i.e. situations in which the species is present or absent in the atmosphere are well separated.*

11. *The factor uncertainties were finely adjusted at the end of the procedure by scaling them so that the residuals fell within the expected range of* ±3*. In this study, an additional 20 % increase in all C_3 values was required. The coefficients were scaled accordingly rather than introducing an additional parameter ('Additional model uncertainty') in EPA PMF 5.0. The C_3 values reported in Table S1 include this factor and their reported digits are approximated to* ±0.05 *for clarity.*

The final values for the parameters A, α, and C_3 are shown in Table S1. [...]

It may be noted that:

- *The uncertainty assigned to the largest size channels ($d > 6\,\mu m$) is relatively high. This reflects the low number concentration of large particles and their 'shot' nature, which introduces greater variability when considered from a Poisson-based perspective (Sect. S2.1). Indeed, these bins typically contain a few peak values emerging from a background of zeros, whose frequency can reach up to 30 %. Consequently, these size channels, together with the total variable PM_{10}, were classified as weak variables in the PMF configuration to prevent them from exerting excessive influence during subsequent tests. During the testing phase, as suggested in previous studies (e.g., Zhou et al., 2004; Thimmaiah et al., 2009; Zhou et al., 2005b), an alternative approach was also evaluated in which the largest size bins were grouped (in sets of three to five, depending on particle size) to mitigate issues associated with low particle counts and to improve the signal-to-noise ratio (SNR). Although bin grouping effectively increased the SNR, it hindered the separation of the two coarse factors (desert dust and local resuspension). For this reason, this approach was not adopted in the final configuration.*

- *The NeBC uncertainties used in this study are lower than those reported in some previous works (e.g., Forello et al., 2019; Rigler et al., 2020). In particular, Forello et al. (2023) applied an uncertainty as high as 50 % for b_{abs} to avoid convergence issues when coupling absorption data with chemical data in the PMF. With such high uncertainty values, combined with the smaller number of optical variables relative to chemical species, the NeBC information effectively follows the factorisation rather than contributing to it. In contrast, the present approach aims to ensure that both spectral absorption and volume size distribution contribute to determining the final solution. Consequently, the uncertainty values adopted here should not be interpreted as strict measurement uncertainties, but rather as weighting parameters used to balance the influence of the different input variables on the Q metric.*

The sentence "no other modelling uncertainty was included" refers to the field Extra Modelling Uncertainty (%) (EMU) available in one of the configuration windows of the EPA PMF software. This parameter allows the user to artificially increase the declared uncertainty of the input data. In the present study, this parameter was not used because the input uncertainties had already been appropriately defined within the uncertainty framework described in Sect. 3.2.1. The sentence has therefore been clarified as follows: *The field Extra Modelling Uncertainty of the EPA PMF was left unchanged (0%).*

In addition, taking the suggestions received in the review process into account, the manuscript has been expanded by including the application of the Effective Variance Least Squares (EVLS) method to RASPBERRY. This method allows the measurement uncertainties of the input data to be fully propagated to the retrievals, together with the uncertainty associated with rotational ambiguity in the profiles. The method is now illustrated and discussed in the revised manuscript.

A clarifying sentence has also been added to Sect. 3.1.2 based on the reviewer's suggestion to anticipate the discussion: *These values refer to the input uncertainties used in the training (PMF) phase of RASPBERRY. A more comprehensive overview of the method limitations and of the overall uncertainties associated with the retrievals is provided in Sects. 3.3 and 5.*

RC2. In line 330, the seasonal balanced sample selection is mentioned, if the samples are not daily, is the diurnal sampling also balanced?

AR2. We thank the reviewer for this comment, and it is true that this detail was not explicitly stated in the original manuscript. This information has now been added to the revised manuscript, Sect. 3.2: *Owing to the continuous 24 h measurement coverage in the original dataset, the random sampling procedure also results in a nearly homogeneous distribution of observations throughout the day. For example, when considering four day-quarter intervals (0–6, 6–12, 12–18, and 18–24 h), the maximum deviation from a uniform distribution is approximately 3 %.*

This is illustrated in Fig. 1 in this document for the reviewer's reference.

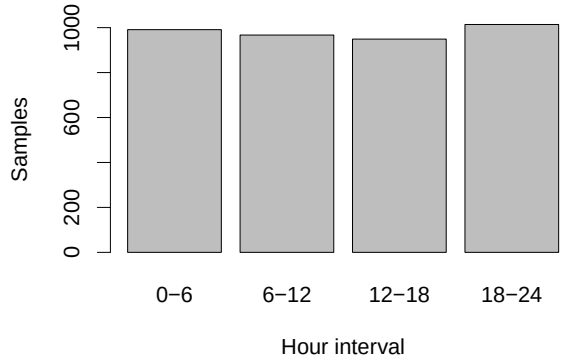

Figure 1: Frequency distribution of samples used for RASPBERRY training across day quarters.

RC3. Line 610, the pink means dust touching the ground in Figs. S24 or in Figure 7? Also is there any lidar to proof that the differences between AERONET and RASPBERRY are due to aloft and surface dust?

AR3. The sentence was modified as follows to avoid confusion (note that the colour description has now been changed to 'yellow', according to a comment by referee #2): *Furthermore, based on the analysis of vertical profiles from the ALCs in Aosta–Saint-Christophe, dust layers that remain primarily aloft (light blue bands in Fig. 7b), detected by the sun photometer but not by the in-situ surface instruments, are discriminated from those that ultimately enter the mixing layer and reach the ground (yellow bands in Fig. 7b). Representative examples are shown using lidar diagrams in Figs. S31a–S31d.*

Co-located automated lidar-ceilometers (ALCs) were indeed used to attribute the observed differences between AERONET and RASPBERRY to dust layers remaining aloft or reaching the surface. The cases

illustrated by the blue and yellow bands were manually verified using the corresponding lidar profiles in order to ensure the robustness of the classification.

RC4. Figure 8a, the differences between chem-PMFd1 and RASPBERRY is very hard to tell due to similar colors. For Fig. 8b, the liner regression cannot represent the true trend of this data. What causes the large scattering in traffic emission contribution? For Secondary rich factors, high bias can be seen throughout, what is the main cause?

AR4. The colours in Fig. 8a were further contrasted to improve readability and facilitate the distinction between chem-PMFd1 and RASPBERRY. The updated plot is reported here as Fig. 2.

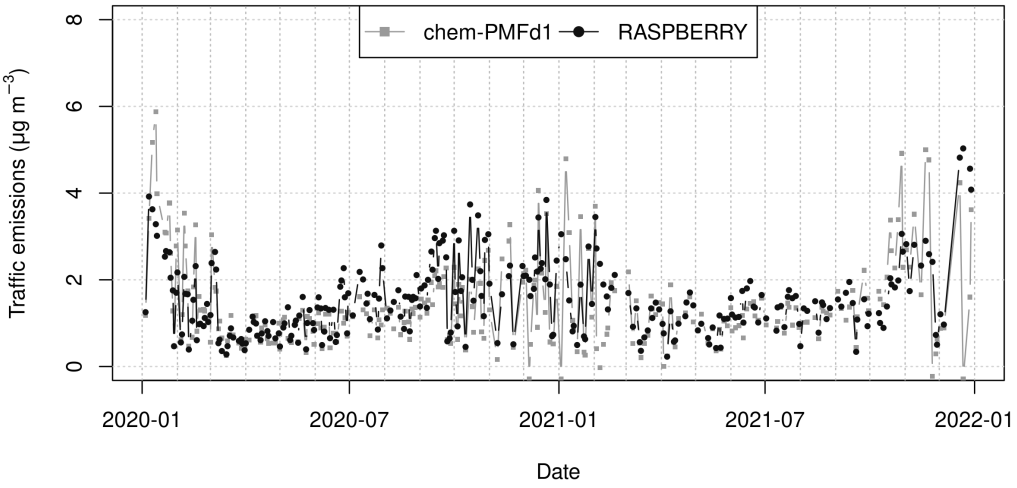

Figure 2: Comparison of daily averaged PM_{10} contribution attributed to traffic derived from the chemical PMF and RASPBERRY.

Regarding the traffic factor, and notably the scattering and the apparent inadequacy of the linear regression, the inclusion of the EVLS method in the revised manuscript provides additional insight into the imperfect agreement between the physical and chemical source apportionment for this source. Indeed, as Aosta is not a large and heavily trafficked city (33,000 inhabitants; Diémoz et al., 2019, 2021), the contributions derived from both the physical and chemical approaches are relatively small and consistently remain below a few $\mu g\,m^{-3}$. At the same time, the relative uncertainty associated with traffic emissions is among the highest of all dimensional profiles. This combination of low signal and comparatively large uncertainty naturally leads to a substantial dispersion in the point-to-point comparison (Fig. 3, complementing the results in Fig. 8b reported in the first version of the manuscript and now included in Fig. S34).

The corresponding paragraph in Sect. 4.3 was therefore updated as follows:

The comparison of traffic factors is depicted in Figs. 8a (time series) and 8b (scatter plot). From the first panel, it is evident that the magnitude of contributions from both source apportionments is about the same, as are the overall seasonal trends. However, the point-to-point relationship illustrated in the second panel reveals some discrepancies, with a Pearson's correlation coefficient of $\rho = 0.67$ *(*$R^2 = 0.45$*). Furthermore, the regression coefficients deviate from the 1:1 line (*$y = 0.58\,x + 0.72\ \mu g\,m^{-3}$*). This deviation can be attributed to difficulties in accurately identifying the traffic factor, primarily due to the following reasons:*

– *Contributions from both source apportionments are relatively low, steadily remaining below 6* $\mu g\,m^{-3}$*,*

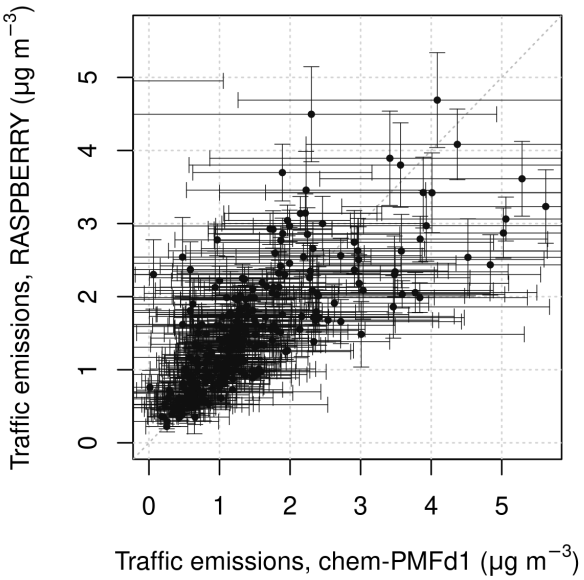

Figure 3: Comparison of daily-averaged PM_{10} source contributions attributed to traffic derived from the chemical PMF (further reprocessed using EVLS) and RASPBERRY+EVLS, shown together with their individual uncertainties. The figure clearly shows that the uncertainty in the chemical source apportionment is larger than in the physical one.

which is consistent with the fact that Aosta is a relatively small, low-traffic city (33,000 inhabitants; Diémoz et al., 2019, 2020, 2021). At the same time, the relative uncertainty associated with traffic emissions is among the highest of all dimensional profiles. This is evident from both the large interval ratio obtained from the DISP test (Sect. 4.2 and Fig. 3) and from the uncertainties derived using the EVLS method for both the physical and the chemical data sets (Fig. S34).

- *The finite lower detection limit of the OPC does not allow all aerosols emitted by traffic to be captured. In particular, most of the studies focusing on ultrafine and accumulation-mode particles (among the most recent examples, Harni et al., 2024; Beddows et al., 2025; Ćirović et al., 2026; Mapelli et al., 2026) identified at least two distinct factors related to traffic (e.g., freshly nucleated vs more aged or distant particles, or gasoline vs diesel/heavy-duty emissions). This may indicate that the physical setup and the chemical analyses effectively 'detect' different factors attributed to traffic.*
- *The coarse resuspended fraction, which significantly contributes to the mass, may be characterised in slightly different amounts in the chemical and the physical source apportionments, as discussed in Sect. S10. Distinguishing unambiguously exhaust and non-exhaust particle contributions is a well-known challenge, frequently reported in the literature (Forello et al., 2023).*
- *The mass absorption cross-section (MAC) in aethalometer measurements may decrease in winter compared to summer, as observed in several studies, e.g. Mousavi et al. (2019) in Milan and Savadkoohi et al. (2024) on a European scale. Such seasonal variation is consistent with an underestimation of NeBC during winter, when concentrations are higher, and an overestimation during summer, when concentrations are lower, in RASPBERRY.*

At the same time, it should be noted that the comparison slope for the traffic factor is higher than 1 when using York and log-transformed York regressions (Table S3), since the intercept decreases. Therefore, the deviation from the 1:1 line may also be partly attributable to an artefact of the regression method itself.

Regarding the secondary-rich factor, the apparent high bias observed in the regression was further analysed to determine whether it represents a systematic data feature or rather depends on the specific regression technique employed. To this end, as already anticipated in the answer above, we recalculated

the regression using several alternative and more advanced approaches, reported in the table below, namely: (i) total least squares (Deming regression; Linnet, 1990), performed by accounting for the actual variance-error ratios obtained from the DISP test of both the physical and chemical PMF solutions; (ii) York regression (York et al., 2004), performed using individual uncertainties calculated through EVLS for both the physical (RASPBERRY+EVLS) and chemical (PMF+EVLS) data sets; and (iii) York regression applied to log-transformed quantities to account for heteroscedasticity in the data.

Table 1: Regression coefficients and their standard errors between the PM_{10} contributions from the chemical PMF (x) and RASPBERRY(+EVLS) (y), determined using different regression methods: ordinary least squares (OLS), Deming regression (total least squares, Linnet, 1990), York regression (York et al., 2004), and log-log York regression to account for heteroscedasticity.

Method	Coefficients	Traffic	Biomass burning	Secondary [a]	Coarse [b]
OLS	Slope	0.58 ± 0.04	0.99 ± 0.02	0.99 ± 0.04	0.95 ± 0.03
	Intercept ($\mu g\,m^{-3}$)	0.72 ± 0.06	0.34 ± 0.04	1.62 ± 0.28	1.36 ± 0.19
Deming [c]	Slope	0.60 ± 0.05	1.08 ± 0.04	1.08 ± 0.05	0.96 ± 0.05
	Intercept ($\mu g\,m^{-3}$)	0.70 ± 0.09	0.22 ± 0.03	1.16 ± 0.24	1.31 ± 0.20
York [d]	Slope	1.35 ± 0.12	1.20 ± 0.03	1.32 ± 0.03	1.58 ± 0.03
	Intercept ($\mu g\,m^{-3}$)	-0.16 ± 0.11	0.12 ± 0.01	0.01 ± 0.12	-0.88 ± 0.08
York (log)	Slope	1.05 ± 0.08	0.86 ± 0.02	1.26 ± 0.04	1.32 ± 0.02
	Intercept ($\mu g\,m^{-3}$)	0.01 ± 0.05	0.32 ± 0.02	-0.51 ± 0.08	-0.41 ± 0.03

[a] Sum of sulfate- and nitrate-rich factors from the chemical PMF, and condensation and droplet mode factors from RASPBERRY.
[b] Sum of road salting and crustal factors from the chemical PMF, and desert dust and local dust resuspension from RASPBERRY, excluding data influenced by significant Saharan dust events.
[c] The regression was performed taking into account the actual variance-error ratios obtained from the DISP test of both physical and chemical PMFs. RASPBERRY retrievals were used with this method.
[d] The regression was performed using individual uncertainties calculated through EVLS for both the physical (RASPBERRY+EVLS) and chemical (PMF+EVLS) data sets (Fig. S34). York et al. (2004) regression yields the same coefficients as those obtained using Python's implementation of orthogonal distance regression (ODR).

The main text was correspondingly updated with the remark: *[...] the large positive intercept for the secondary factors is statistically significant when using OLS and Deming regressions, but not with York regression, and it turns negative (and statistically significant) when York regression is applied to log-transformed data. This result suggests that, similarly to traffic, the apparent high bias is largely an artefact of the regression method, and perhaps of the heteroscedastic nature of the data, rather than a systematic discrepancy between the two source apportionment approaches.*

RC5. Figure 13 e and f, the vertical level where backscattering shows smoke, does not have valid retrieval of depolarization ratio in g and h. (For example, the small chunk of smoke at 5km in 13f, the location is corresponding to noise/no-retrieval for 13h.)

AR5. The reviewer is correct. This limitation has now been clarified in the revised manuscript. Specifically, we state: *It should be noted that aerosol depolarisation measurements obtained with the CL61 generally exhibit low signal-to-noise ratios, particularly for elevated and optically thin layers (Looschelders et al., 2025). Consequently, the smoke layers identified in the backscatter profiles (Figs. 13e–f) cannot be robustly characterised in terms of their depolarisation properties.* The figure caption has also been up-

dated accordingly: *Note that, in this case, the low smoke depolarisation, together with the weak signal-to-noise ratio of the CL61, limits reliable depolarisation measurements to the lowest atmospheric layers.* In addition, we have improved the visualisation by applying a more accurate mask based on the signal-to-noise ratio of the backscatter coefficient, and particle depolarisation ratio is now shown instead of volume depolarisation ratio, ensuring consistency with recent literature.

References

Aujay-Plouzeau, R.: Guide méthodologique pour la mesure du «Black Carbon» par Aethalomètre multi longueur d'onde AE33 dans l'air ambiant (Version 2020), Tech. rep., Ineris, https://www.lcsqa.org/system/files/media/documents/LCSQA2019-Guide_mesure_BlackCarbon_par_AE33_VF03-Approuv%C3%A9CPS15122020.pdf, 2020.

Beddows, D., Brean, J., Rowell, A., Merkel, M., Weinhold, K., Dall'Osto, M., and Harrison, R.: Wide-Positive Matrix Factorisation of particle number size distributions: A new approach accounting for cyclically changing source profiles, Sci. Total Environ., 998, 180 231, https://doi.org/10.1016/j.scitotenv.2025.180231, 2025.

Ćirović, Ž., Stojanović, D. B., Davidović, M., Onjia, A., Alastuey, A., and Jovašević-Stojanović, M.: New Particle Formation and Source Apportionment of Particle Number Size Distribution in the Urban Area of the City of Belgrade, Atmosphere, 17, https://doi.org/10.3390/atmos17020205, 2026.

Diémoz, H., Gobbi, G. P., Magri, T., Pession, G., Pittavino, S., Tombolato, I. K. F., Campanelli, M., and Barnaba, F.: Transport of Po Valley aerosol pollution to the northwestern Alps – Part 2: Long-term impact on air quality, Atmos. Chem. Phys., 19, 10 129–10 160, https://doi.org/10.5194/acp-19-10129-2019, 2019.

Diémoz, H., Tombolato, I. K. F., Zublena, M., Magri, T., and Ferrero, L.: The impact of biomass burning emissions on PM concentration in the Greater Alpine region, in: Proceedings of 12th International Conference on Air Quality, Science and Application, p. 26, Hatfield, UK, 10.18745/pb.22217, 2020.

Diémoz, H., Magri, T., Pession, G., Tarricone, C., Tombolato, I. K. F., Fasano, G., and Zublena, M.: Air Quality in the Italian Northwestern Alps during Year 2020: Assessment of the COVID-19 «Lockdown Effect» from Multi-Technique Observations and Models, Atmosphere, 12, https://doi.org/10.3390/atmos12081006, 2021.

Forello, A. C., Bernardoni, V., Calzolai, G., Lucarelli, F., Massabò, D., Nava, S., Pileci, R. E., Prati, P., Valentini, S., Valli, G., and Vecchi, R.: Exploiting multi-wavelength aerosol absorption coefficients in a multi-time resolution source apportionment study to retrieve source-dependent absorption parameters, Atmos. Chem. Phys., 19, 11 235–11 252, https://doi.org/10.5194/acp-19-11235-2019, 2019.

Forello, A. C., Cunha-Lopes, I., Almeida, S. M., Alves, C. A., Tchepel, O., Crova, F., and Vecchi, R.: Insights on the combination of off-line and on-line measurement approaches for source apportionment studies, Sci. Total Environ., 900, 165 860, https://doi.org/10.1016/j.scitotenv.2023.165860, 2023.

Gu, J., Pitz, M., Schnelle-Kreis, J., Diemer, J., Reller, A., Zimmermann, R., Soentgen, J., Stoelzel, M., Wichmann, H.-E., Peters, A., and Cyrys, J.: Source apportionment of ambient particles: Comparison of positive matrix factorization analysis applied to particle size distribution and chemical composition data, Atmos. Environ., 45, 1849–1857, https://doi.org/10.1016/j.atmosenv.2011.01.009, 2011.

Harni, S. D., Aurela, M., Saarikoski, S., Niemi, J. V., Portin, H., Manninen, H., Leinonen, V., Aalto, P., Hopke, P. K., Petäjä, T., Rönkkö, T., and Timonen, H.: Source apportionment of particle number size distribution at the street canyon and urban background sites, Atmos. Chem. Phys., 24, 12 143–12 160, https://doi.org/10.5194/acp-24-12143-2024, 2024.

Linnet, K.: Estimation of the linear relationship between the measurements of two methods with proportional errors, Stat. Med., 9, 1463–1473, https://doi.org/10.1002/sim.4780091210, 1990.

Looschelders, D., Christen, A., Grimmond, S., Kotthaus, S., Fenner, D., Dupont, J.-C., Haeffelin, M., and Morrison, W.: Inter-Instrument Variability of Vaisala CL61 Lidar-Ceilometer's Attenuated Backscatter, Cloud Properties and Mixed-Layer Height, Meteorol. Appl., 32, e70 088, https://doi.org/10.1002/met.70088, 2025.

Mapelli, C., Diémoz, H., Contini, D., Dinoi, A., Cesari, D., and Barnaba, F.: Physics-based aerosol source apportionment at the site of Lecce (Italy), Atmos. Res. (under review), 2026.

Mousavi, A., Sowlat, M. H., Lovett, C., Rauber, M., Szidat, S., Boffi, R., Borgini, A., De Marco, C., Ruprecht, A. A., and Sioutas, C.: Source apportionment of black carbon (BC) from fossil fuel and biomass burning in metropolitan Milan, Italy, Atmos. Environ., 203, 252–261, https://doi.org/10.1016/j.atmosenv.2019.02.009, 2019.

Norris, G., Duvall, R., and Brown, S.: EPA Positive Matrix Factorization (PMF) 5.0 Fundamentals and User Guide, U.S. Environmental Protection Agency Office of Research and Development Washington, DC 20460, `https://www.epa.gov/sites/default/files/2015-02/documents/pmf_5.0_user_guide.pdf`, ePA/600/R-14/108, 2014.

Ogulei, D., Hopke, P. K., Zhou, L., Pancras, J. P., Nair, N., and Ondov, J. M.: Source apportionment of Baltimore aerosol from combined size distribution and chemical composition data, Atmos. Environ., 40, 396–410, https://doi.org/10.1016/j.atmosenv.2005.11.075, 2006.

Ogulei, D., Hopke, P. K., Chalupa, D. C., , and Utell, M. J.: Modeling Source Contributions to Submicron Particle Number Concentrations Measured in Rochester, New York, Aerosol Sci. Tech., 41, 179–201, https://doi.org/10.1080/02786820601116012, 2007.

Rigler, M., Drinovec, L., Lavrič, G., Vlachou, A., Prévôt, A. S. H., Jaffrezo, J. L., Stavroulas, I., Sciare, J., Burger, J., Kranjc, I., Turšič, J., Hansen, A. D. A., and Močnik, G.: The new instrument using a TC–BC (total carbon–black carbon) method for the online measurement of carbonaceous aerosols, Atmos. Meas. Tech., 13, 4333–4351, https://doi.org/10.5194/amt-13-4333-2020, 2020.

Savadkoohi, M., Pandolfi, M., Favez, O., Putaud, J.-P., Eleftheriadis, K., Fiebig, M., Hopke, P. K., Laj, P., Wiedensohler, A., Alados-Arboledas, L., Bastian, S., Chazeau, B., Álvaro Clemente María, Colombi, C., Costabile, F., Green, D. C., Hueglin, C., Liakakou, E., Luoma, K., Listrani, S., Mihalopoulos, N., Marchand, N., Močnik, G., Niemi, J. V., Ondráček, J., Petit, J.-E., Rattigan, O. V., Reche, C., Timonen, H., Titos, G., Tremper, A. H., Vratolis, S., Vodička, P., Funes, E. Y., Zíková, N., Harrison, R. M., Petäjä, T., Alastuey, A., and Querol, X.: Recommendations for reporting equivalent black carbon (eBC) mass concentrations based on long-term pan-European in-situ observations, Environ. Int., 185, 108 553, https://doi.org/10.1016/j.envint.2024.108553, 2024.

Thimmaiah, D., Hovorka, J., and Hopke, P. K.: Source apportionment of winter submicron prague aerosols from combined particle number size distribution and gaseous composition data, Aerosol Air Qual. Res., 9, 209–236, https://doi.org/10.4209/aaqr.2008.11.0055, 2009.

Vörösmarty, M., Hopke, P. K., and Salma, I.: Attribution of aerosol particle number size distributions to main sources using an 11-year urban dataset, Atmos. Chem. Phys., 24, 5695–5712, https://doi.org/10.5194/acp-24-5695-2024, 2024.

York, D., Evensen, N. M., Martínez, M. L., and De Basabe Delgado, J.: Unified equations for the slope, intercept, and standard errors of the best straight line, Am. J. Phys., 72, 367–375, https://doi.org/10.1119/1.1632486, 2004.

Zhou, L., Hopke, P. K., Paatero, P., Ondov, J. M., Pancras, J., Pekney, N. J., and Davidson, C. I.: Advanced factor analysis for multiple time resolution aerosol composition data, Atmos. Environ., 38, 4909–4920, https://doi.org/10.1016/j.atmosenv.2004.05.040, 2004.

Zhou, L., Hopke, P. K., Stanier, C. O., Pandis, S. N., Ondov, J. M., and Pancras, J. P.: Investigation of the relationship between chemical composition and size distribution of airborne particles by partial least squares and positive matrix factorization, J. Geophys. Res., 110, https://doi.org/10.1029/2004JD005050, 2005a.

Zhou, L., Kim, E., Hopke, P. K., Stanier, C., and Pandis, S. N.: Mining airborne particulate size distribution data by positive matrix factorization, J. Geophys. Res., 110, https://doi.org/10.1029/2004JD004707, 2005b.